

Command Shaping for Sloshing Suppression of a Suspended Liquid Container

Abdullah Alshaya¹

Mechanical Engineering Department,
Kuwait University,
P.O. Box 5969,
Safat 13060, Kuwait
e-mail: abdullah.alshaye@ku.edu.kw

Khalid Alghanim

Mechanical Engineering Department,
Kuwait University,
P.O. Box 5969,
Safat 13060, Kuwait
e-mail: khalid.ghanim@ku.edu.kw

The residuals of liquid free-surface wave oscillations induced by a rest-to-rest crane maneuver of a suspended liquid container are eliminated using a command-shaped profile. The dynamics of liquid sloshing are modeled using an equivalent mechanical model based on a series of mass-spring-damper systems. The proposed model considers the excited frequencies of the container swing motion and liquid sloshing modes. The objective is to design a discrete-time shaped acceleration profile with a variable command length that controls the moving crane-jib, while suppressing the sloshing modes. Simulations are conducted to illustrate the command effectiveness in eliminating liquid sloshing with a wide variation range of system and command-designing parameters; liquid depth, cable length, command duration, and the employing of higher sloshing modes in representing the sloshing dynamics. The command sensitivity of the input command to changes of the system parameters are treated as well. A refined and smooth input command based on suppressing the residuals of multimodes is also introduced. Furthermore, the command effectiveness was supported by a comparison with the time-optimal flexible-body control and multimode zero vibration input shaper. [DOI: 10.1115/1.4047957]

Keywords: vibration control, sloshing suppression, command-shaping, overhead crane, open-loop control

1 Introduction

Robotic manipulators and overhead, or gantry, cranes are used extensively to move containers in repeated cycles. Optimal control techniques are necessary in minimizing residual vibrations during a move cycle, while minimizing move time. A cycle, or a point-to-point maneuver, is composed of acceleration, cruising and deceleration stages. It is only practical if residual vibrations are dissipated before a second motion is introduced.

Typically, containers are moved with a sufficiently low acceleration, lower than the system's capability, as to not induce any vibration; otherwise, the induced vibration will result in idling the operation while waiting for the vibration to decay. When an overhead crane is used to transport liquids in point-to-point maneuvers, the rapid excitation of the inside liquid induces sloshing during the maneuvers. Liquid sloshing could cause fatigue on the container structure leading to accidents. Excessive liquid sloshing may also cause spillage, more critically, of hazardous substances such as molten metal. Moreover, excessive sloshing can cause the system to become unstable. With a proper control technique, the maneuver can be completed in a shorted time period while maintaining minimal levels of residual vibrations.

Recently, controlling the oscillations induced by the motion of a liquid container attracts the attention of many researchers [1–11]. Using passive methods such as absorbers and baffles to dissipate sloshing increases the weight and adds complexity to the overall system [12,13]. Alternatively, there are several active control techniques, e.g., linear-quadratic-integral, H^∞ , and input shaping, that have been proposed, simulated, and tested to suppress sloshing in a moving liquid-filled container. The requirement of liquid-motion sensors renders difficulties in implementing traditional feedback controllers. Alternatively, without using sensors, input shaping technique was successfully utilized to move containers with minimal transient and residual liquid oscillations

[5,6,8]. Input shaping is based on convolving a general reference command signal with sequences of specified timed-impulses that generates a specially shaped command to reduce residual vibrations. Pioneer works in input shaping techniques are given in Refs. [14–18]. Input shapers can reside completely outside a control system and, therefore, can be easily integrated with other control schemes. The most drawbacks of the input shaping are the high sensitivity to variations of the modeling errors and system parameters and the prior knowledge of the system dynamics.

In general, a sloshing problem in containers is highly characterized by a nonlinear coupled system [19]. However, under a horizontal excitation of a rectangular container with small oscillations, the sloshing dynamics can be modeled based on spring-mass systems [20]. Yano and Terashima [2] suppressed sloshing using a feedback controller and an equivalent simple pendulum system to represent the sloshing dynamics. For a rectangular container being moved in a horizontal direction, the induced sloshing was eliminated using input commands while modeling the sloshing dynamics using the finite-element method for the liquid–structure interactions [3] and an equivalent mechanical model [6]. Hunag and Zaho [11] suppressed sloshing while the rectangular container is moving along the lateral and transverse directions. Murthy et al. [5] and AlSaibie and Singhose [8] suppressed sloshing in a suspended container using different input shaping methods. However, they used the natural frequencies of a liquid container excited by lateral motion and neglected the rotation effect induced by the crane. Kaneshige et al. [4] utilized notch filter control to suppress sloshing in an overhead crane system.

The aim of this work is to design a shaped command with adjustable command length that suppresses the sloshing residuals of a suspended liquid container. The input command based on a series of steps is designed to produce fast maneuvering and accurate positioning. Numerical simulations are conducted to illustrate the command effectiveness and robustness. The variation of system parameters such as changing the liquid level and cable length in the command performance is also addressed. A refined and smooth input command based on multisteps (introducing higher sloshing modes) is also proposed for further application. Unlike the works by Murthy et al. [5] and AlSaibie and Singhose [8]

¹Corresponding author.

Contributed by the Dynamic Systems Division of ASME for publication in the JOURNAL OF DYNAMIC SYSTEMS, MEASUREMENT, AND CONTROL. Manuscript received October 13, 2019; final manuscript received June 30, 2020; published online August 28, 2020. Assoc. Editor: Weichao Sun.

where they used the common input shapers, zero-vibration and zero-vibration-derivative, for reducing the residual sloshing in a moving container, the proposed command guarantees the elimination of residual sloshing by using a multisteps input command (MSIC) that captures the multimodal response of the liquid with adjustable command length. The effectiveness of the proposed command was supported by a comparison with the time-optimal flexible-body control and multimode zero vibration input shaper.

The paper is organized into five major sections. A mathematical model to simulate the dynamics of the suspended liquid system under investigation is formulated in Sec. 2. The system constraints in designing the input command are addressed in Sec. 3. In Sec. 4, a conducted numerical simulation and its corresponding results are presented. Finally, the conclusions of this work are given in Sec. 5.

2 Mathematical Model

A partially filled liquid container conveyed by an overhead crane is shown in Fig. 1(a). A realistic representation of the liquid sloshing dynamics inside a rigid-walled container can be approximated by an equivalent mechanical model consisting of mass-spring-damper systems. Each of these damped harmonic oscillators in Fig. 1(b) represents one of the vibratory modes of the liquid sloshing. The slider (jib) moves horizontally with a proposed predefined acceleration command shaper profile.

The liquid sloshing can be excited by a combination of lateral and vertical motions due to angular motion. The sloshing dynamics are assumed to be induced only by the lateral motions. For simplicity, the nonlinearity of sloshing dynamics under combined excitation including heaving and pitching is neglected.

2.1 Mechanical Model of Sloshing Dynamics. For a linear planar liquid motion without rotation and with the excitation frequency remote from resonance, an equivalent mechanical model in the form of a series of mass-spring-damper systems or a set of simple pendulums in the sense of equal resulting forces and moments acting on the container can be developed to provide a realistic representation of the liquid free-surface dynamics [19,20]. If the container is oscillated near the surface wave resonance frequency, linear modeling is no longer valid and nonlinear

representation must be considered since jumps can be observed [21].

2.2 Governing Equations. A simplified model of an overhead crane is shown in Fig. 1. The model consists of a rigid-walled container of mass m_c , width W (in the direction of wave motion), height H , and mass moment of inertia I_c (with respect to its own center of mass) that is filled with a liquid of filling level h . The inside liquid is modeled by a moment of inertia I_0 assigned to a rigidly attached mass, m_0 , that moves with the container and n lumped, point, masses m_i ($i = 1, 2, \dots, n$) attached to the container's wall by means of springs and dampers that simulate the dynamics of the liquid sloshing. Figure 1(b) shows the equivalent mechanical model that represents the liquid free-surface oscillations where m_i , k_i , and c_i denote the equivalent mass, the equivalent spring stiffness constant, and the equivalent viscous damper constant of the i th sloshing mode, respectively; h_i denotes the distance from the liquid center of mass, $h/2$ (in its undistributed condition) to the equivalent i th mass point, m_i ; and h_0 is the distance from the liquid center to the rigid mass, m_0 . The equivalent viscous coefficient c_i considers the viscosity of the liquid and the friction between the liquid and the wall. The parameters $m_0, I_0, h_0, m_i, h_i, k_i, c_i$ of the equivalent mechanical model depend on the shape of the container, the liquid filling ratio, h/W , of the container, and the characteristic of the liquid [19]. The advantage of using an equivalent mechanical model of sloshing dynamics is to facilitate the designing process in controlling the suspended liquid system. The adopted mechanical model used herein is from Ref. [20] where the corresponding model parameters are given in Eq. (A1) in the Appendix A.

The container is attached to a jib by means of a massless cable of length a . The jib moves in the horizontal direction with acceleration $\ddot{u}(t)$, while the container swings in the xy -plane with an oscillation angle $\theta(t)$. Each lumped mass, m_i , moves along the container-fixed lateral axis with a relative displacement $q_i(t)$ ($i = 1, 2, \dots, n$) with respect to the container's wall, Fig. 1(a). Each coordinate q_i represents the motion of the liquid surface corresponding to the i th sloshing mode. The elevation of the liquid free-surface level is given by [11]

$$\eta(x, y, t) = \sum_{i=1}^n \phi_i(x, y) q_i(t) \quad (1)$$

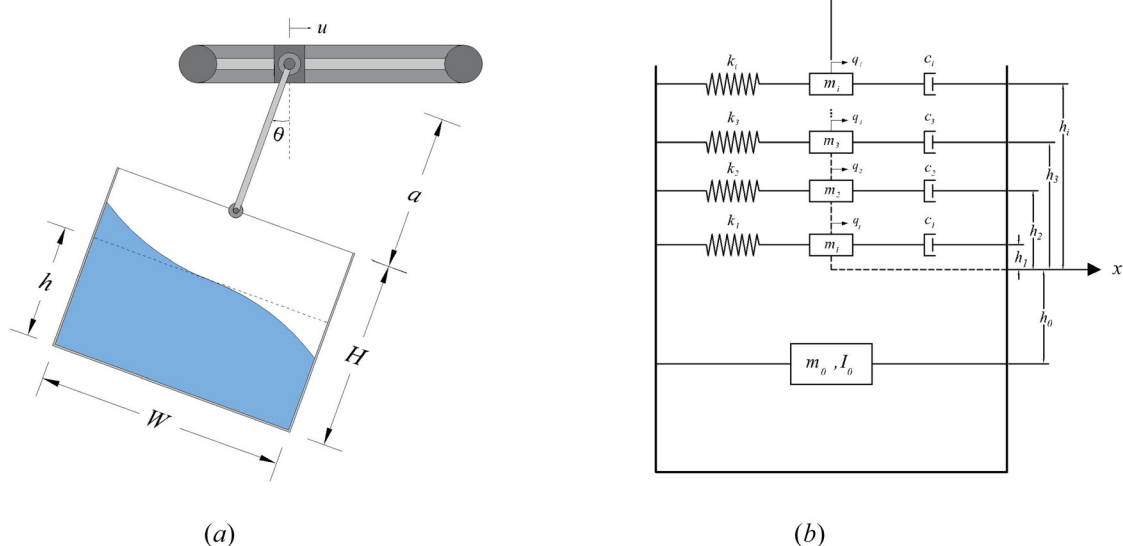


Fig. 1 (a) A rigid-walled container filled by a liquid and conveyed by an overhead crane and (b) equivalent mechanical model of the liquid sloshing modes

where $\phi_i(x, y)$ represents the i th sloshing spatial mode function. The spillage is most likely to occur at the edges of the container, i.e., $x = \pm W/2$ and $y = 0$. Therefore, the wave motion of the liquid surface, $\delta(t)$, as a function of time at the edge is the sum of the surface wave oscillations of each of the sloshing modes

$$\delta(t) = \eta(\pm W/2, 0, t) = \sum_{i=1}^n \phi_i(\pm W/2, 0) q_i(t) \quad (2)$$

Upon defining the position vectors of the container's center of mass, the liquid fixed-mass, m_0 , and the i th point mass, m_i , taking the time derivatives to obtain the velocity vectors, stating the kinetic, potential, and Rayleigh dissipation energies of the liquid suspended system, and employing Lagrange's formulation, the following fully coupled nonlinear differential equations in angular coordinate, θ , and the lateral displacements, q_i , were obtained:

$$\begin{aligned} & \left[I_{eq} + \sum_{i=1}^n m_i q_i^2 \right] \ddot{\theta} - \sum_{i=1}^n m_i l_i \ddot{q}_i + 2 \left[\sum_{i=1}^n m_i q_i \dot{q}_i \right] \dot{\theta} \\ & + \left[M_l \sin \theta - \cos \theta \sum_{i=1}^n m_i q_i \right] g \\ & = \left[M_l \cos \theta + \sin \theta \sum_{i=1}^n m_i q_i \right] \ddot{u} \end{aligned} \quad (3a)$$

$$\begin{aligned} & -l_i \ddot{\theta} + \ddot{q}_i - q_i \dot{\theta}^2 + 2\zeta \omega_i \dot{q}_i - g \sin \theta + \omega_i^2 q_i = -\cos \theta \ddot{u} \quad \text{for} \\ & i = 1, 2, \dots, n \end{aligned} \quad (3b)$$

where $l_c = a + H/2$, $l_0 = a + H - h/2 + h_0$, and $l_i = a + H - h/2 - h_i$ are the distances from the jib to the container's center of mass, the liquid fixed-mass, m_0 , and the i th lumped mass, m_i , respectively, g is gravitational constant, ζ and ω_i are the damping ratio of the fluid and natural frequency of the mass-spring system, respectively, and

$$\begin{aligned} I_{eq} &= I_c + m_c l_c^2 + I_0 + m_0 l_0^2 + \sum_{i=1}^n m_i l_i^2 \quad \text{and} \\ M_l &= m_c l_c + m_0 l_0 + \sum_{i=1}^n m_i l_i \end{aligned}$$

The dissipative term $2 \sum_{i=1}^n m_i q_i \dot{q}_i \dot{\theta}$ in Eq. (3a) represents the damping force from the liquid into the container's walls. The $n+1$ equations of motion, (3), are subjected to the following initial conditions:

$$\theta(0) = \theta_0, \quad \dot{\theta}(0) = \dot{\theta}_0 \quad (4a)$$

$$q_i(0) = q_{i,0}, \quad \dot{q}_i(0) = \dot{q}_{i,0} \quad \text{for } i = 1, 2, \dots, n \quad (4b)$$

where θ_0 and $\dot{\theta}_0$ are the initial oscillation angle and rotational speed of the cable, a , and q_i and \dot{q}_i are the initial relative displacement and velocity of the lumped mass m_i with respect to the container's wall. For completeness, the initial conditions are included in the theoretical derivation, even though the proposed command will be designed to convey the suspended system from its rest state, i.e., zero initial conditions.

2.3 General Solution of a Multisteps Input Command. The nonlinear Eq. (3) can be linearized by assuming small oscillation angle θ and small surface wave oscillations, q_i . Neglecting the higher-order terms, Eq. (3) is reduced to

$$I_{eq} \ddot{\theta} - \sum_{i=1}^n m_i l_i \ddot{q}_i + M_l g \theta - g \sum_{i=1}^n m_i q_i = M_l \ddot{u} \quad (5a)$$

$$-l_i \ddot{\theta} + \ddot{q}_i + 2\zeta \omega_i \dot{q}_i - g \theta + \omega_i^2 q_i = -\ddot{u} \quad \text{for } i = 1, 2, \dots, n \quad (5b)$$

with the initial conditions given in Eq. (4). A multisteps input command of m steps with amplitudes A_i is proposed

$$\ddot{u}(t) = \sum_{i=1}^m (A_i - A_{i-1}) H_{\tau_i}, \quad \text{with } A_0 = 0 \quad (6)$$

where $H_{\tau_i} = H(t - \tau_i)$ is the Heaviside function. Substitution of Eq. (6) into Eq. (5) and using Laplace transform approach give the general solutions of the multisteps input $\ddot{u}(t)$

$$\theta(t) = \sum_{j=1}^{2n+2} a_j e^{\sigma_j t} + \sum_{k=1}^m \left[\left(\sum_{j=1}^{2n+2} c_j e^{\sigma_j (t-\tau_k)} + c_{2n+3} \right) (A_k - A_{k-1}) H_{\tau_k} \right] \quad (7)$$

$$\begin{aligned} q_i(t) &= \sum_{j=1}^{2n+2} b_{i,j} e^{\sigma_j t} \\ &+ \sum_{k=1}^m \left[\left(\sum_{j=1}^{2n+2} d_{i,j} e^{\sigma_j (t-\tau_k)} + d_{i,2n+3} \right) (A_k - A_{k-1}) H_{\tau_k} \right] \quad \text{for} \\ & i = 1, 2, \dots, n \end{aligned} \quad (8)$$

where a_j , $b_{i,j}$, c_j , and $d_{i,j}$ are complex coefficients and σ_j are the characteristic polynomials. Appendix B contains the definitions and expressions of these coefficients and polynomials. Appendix C provides the stability proof of the system given in Eq. (3) based on Lyapunov theorem.

3 Command Shaping

Command shaping, a commonly used input shaping technique, is an open-loop control technique that is designed to induce minimal transient (when the container is in motion) and residual (when the container is stopped) liquid oscillations. An input command of sequence steps can be generated by convolving a step reference command with a sequence of specified timed impulses. The parameters of this steps input command, namely, the magnitudes of the necessary commanded steps A_i and their timing τ_i , are determined based on the formulated dynamics equations that drive the jib from one point to another while achieving certain prescribed time domain specifications. The presence of nonlinearities of the system in Eq. (3) complicates the designing process of the input command. Therefore, with the fact that sloshing may be modeled as a multi-mode linear system, Eq. (5) was alternatively used in designing the input command. Once the input command is designed, the dynamics responses of the system were obtained from the nonlinear model, Eq. (3). Throughout the paper, the time intervals of the acceleration, cruising, and deceleration stages are denoted, respectively, by t_a , t_c , and t_d .

Two important factors should be considered when designing control commands to suppress liquid oscillations for a system with sloshing dynamics; number of sloshing modes and liquid depth. Some applications require only considering the first mode of sloshing whereas other applications may require the consideration of higher modes. The variation of liquid depth changes the sloshing frequencies during motion. The effect of retaining different sloshing modes and the effect of changing the liquid depth will be deliberately considered in the subsequent sections.

3.1 Command Designing. The input shapers are usually designed from the system natural frequencies and damping ratios. The unavailability of the latter in Eq. (3) renders impossible to determine such shaper that produces zero vibrations using traditional techniques. To ensure having zero residual vibrations at the end of the acceleration stage, the angle θ and the wave surface amplitude δ , Eq. (2), and their derivatives, should be set to zero. Therefore, the input command profile, \ddot{u} , is designed by satisfying the following conditions:

$$\begin{aligned} \theta(t_a) &= 0, \quad \dot{\theta}(t_a) = 0, \quad \delta(t_a) = 0, \quad \dot{\delta}(t_a) = 0, \\ \int_0^{t_a} \ddot{u} &= v_f, \quad |\ddot{u}| \leq a_{\max} \end{aligned} \quad (9)$$

where the first four equality constraints ensure that the system produces zero vibrations at the end of the acceleration stage; the next constraint ensures that the jib reaches its maximum velocity v_f ; and the inequality constraint ensures that the maximum acceleration of the input command does not exceed a predefined value, a_{\max} . The input command should utilize the full system acceleration and velocity capabilities to achieve an optimum maneuver time, $T = t_a + t_c + t_d$. The equality constraints in Eq. (9) produce $2n + 3$ equations. Knowing that to satisfy $\delta(t_a) = 0$ all n wave surface motions $q_i(t_a)$ need to be diminished according to Eq. (2).

The fundamental idea of input shaping is to find the switching intervals and their corresponding impulse magnitudes that are optimal based on the existing natural frequencies and damping ratios of the system [18]. Unlike the classical input shaping techniques, this work proposes a multisteps input command with piecewise constant time segments, $\Delta\tau$, where the time segment, i.e., command length, is independent of the system natural frequencies and the damping ratio. Therefore, one can select an appropriate command length to compensate between the maneuver time and transient oscillation. However, the shortest command length is limited by the maximum allowable command amplitude.

In order to satisfy all the equality constraints in Eq. (9) and in addition to ensure that $|A_i| < a_{\max}$, at least $m = 2n + 3$ steps are needed. Substituting $t = t_a$ into Eqs. (7) and (8) and their time derivatives with the assumption of zero initial conditions, and integrating Eq. (6) from 0 to t_a yield a linear system of $m = 2n + 3$ equations, $\mathbf{Ac} = \mathbf{b}$, that can be solved for the steps amplitudes A_i that satisfy all the equality constraints in Eq. (9). The $m \times m$ matrix \mathbf{A} and m -vectors \mathbf{c} and \mathbf{b} are defined as follows:

$$\begin{aligned} \mathbf{A}(1, k) &= \sum_{j=1}^{2n+2} c_j e^{\sigma_j(t_a - \tau_k)} + c_{2n+3} \\ \mathbf{A}(2, k) &= \sum_{j=1}^{2n+2} \sigma_j c_j e^{\sigma_j(t_a - \tau_k)} \end{aligned} \quad (10a)$$

$$\mathbf{A}(2i+1, k) = \sum_{j=1}^{2n+2} d_{i,j} e^{\sigma_j(t_a - \tau_k)} + d_{i,2n+3} \quad (10b)$$

$$\mathbf{A}(2i+2, k) = \sum_{j=1}^{2n+2} \sigma_j d_{i,j} e^{\sigma_j(t_a - \tau_k)} \quad i = 1, 2, \dots, n \quad (10b)$$

$$\mathbf{A}(2n+3, k) = m - k + 1 \quad k = 1, 2, \dots, m$$

$$\mathbf{c} = \{ A_1 A_2 - A_1 \cdots A_m - A_{m-1} \}^T$$

$$\mathbf{b} = \{ 0 \ 0 \cdots 0 \ v_f / \Delta\tau \}^T \quad (10c)$$

The magnitudes of the steps in the deceleration phase are basically the inversion of those in the acceleration stage. To ensure that the jib moves a certain traveled distance, d , the cruising distance is adjusted once the traveled distance in the acceleration and deceleration stages is determined. The total traveled time, T , is then

evaluated by numerically integrating the velocity profile of the input command.

The magnitudes of the steps determined from Eq. (10) are for the case that the suspended container was conveyed from its rest position to a final rest position. If the water level and swing angle can be recorded in a real-time measurement, the vector \mathbf{b} should be adjusted by adding the first term in the Eqs. (7) and (8). The two constants a_j and $b_{i,j}$ are both functions of the initial conditions embedded in the constants A, B, C_i , and D_i and the polynomials $\mu(s)$ and $\nu_i(s)$ as defined in Appendix B. If a shaped command designed based on zero initial conditions was used to convey the suspended system with nonzero initial states, these initial disturbance will remain as residual vibration at the end of the maneuver (as will be shown later).

3.2 Time-Optimal of Rigid-Body Motion. For comparison, the response of time-optimal of rigid-body (TORB) is considered as the reference case of the unshaped (uncontrolled) command. TORB is the fastest possible input command which utilizes the maximum acceleration to move the jib from its rest position to its maximum cruising speed at the end of the acceleration stage. Once the jib covers the cruising stage, the TORB command will decelerate the jib using its maximum deceleration value to stop the jib at the target position. The time intervals of the acceleration and deceleration stages are equal to $t_a = t_d = v_f/a_{\max}$; the time interval of the cruising stage is $t_c = d/v_f - v_f/a_{\max}$; and therefore, the total traveled time is $T = d/v_f + v_f/a_{\max}$.

4 Simulation Results

For the simulation experiment, the kinematics of the jib, container dimensions, and liquid properties are listed in Table 1. The equivalent lumped masses, spring constants, and damping constants of the vibratory modes of the liquid sloshing are obtained from Eqs. (A1) in Appendix A. The water damping ratio is taken as $\zeta = 0.01$ based on the experimentally determined values [2,6,8] and approximation of an analytical expression [22]. Different liquid filling ratios, h/W , were used to ascertain the effect of liquid levels in the controlling techniques. The coupled nonlinear differential Eq. (3) were solved numerically.

4.1 Response of Time-Optimal of Rigid-Body. The dynamics responses, $\theta(t)$ and $\delta(t)$, of the suspended system subjected to TORB motion using the nonlinear equations of motion, Eq. (3), and the linearized form, (5), are illustrated in Fig. 2 for different sloshing modes. For the given jib kinematics in Table 1, the time interval of TORB motion is $T = 2.33$ s. The maximum swing angle of the TORB (uncontrolled shape) is within the acceptable range of the linearity assumption. Therefore, the nonlinearity behavior of the suspended system can be neglected and the dynamics of the system can be obtained from the linear form, Eq. (5).

Table 1 Jib kinematics, container dimensions, and liquid properties of the numerical simulation

Container dimensions	Value	Container properties	Value
Width, W (cm)	25	Mass, m_c (kg)	10
Height, H (cm)	50	Mass moment	
Cable length, a (cm)	30	of inertia, I_c ($\text{kg} \cdot \text{m}^2$)	0.01
Jib kinematics		Liquid (water) parameters	
Travel distance, d (m)	0.6	Mass density, ρ (kg/m^3)	1000
Maximum velocity, v_f (m/s)	0.3	Damping ratio, ζ	0.01
Maximum acceleration, a_{\max} (m/s^2)	0.9	liquid filling levels, h (cm)	2.5, 5, 15, 20

Table 2 Amplitudes of the input steps, the RMS wave surface oscillations, and the total maneuver time using different time-steps, $\Delta\tau$, single sloshing mode and $h/W=0.1$

		$\Delta\tau = 0.24 \text{ s}$ and $t_a = 1.2 \text{ s}$		$\Delta\tau = 0.30 \text{ s}$ and $t_a = 1.5 \text{ s}$		$\Delta\tau = 0.35 \text{ s}$ and $t_a = 1.75 \text{ s}$									
Amplitudes, $A_k (\text{m/s}^2)$	0.6544	-0.4807	0.8958	-0.4412	0.6218	$\Psi (\text{mm})$	3.53	Times, $\tau_k (\text{s})$	0.00	0.24	0.48	0.72	0.96	$T (\text{s})$	3.19
		$\Delta\tau = 0.30 \text{ s}$ and $t_a = 1.5 \text{ s}$		$\Delta\tau = 0.35 \text{ s}$ and $t_a = 1.75 \text{ s}$											
Amplitudes, $A_k (\text{m/s}^2)$	0.2656	0.1149	0.2421	0.1283	0.2491	$\Psi (\text{mm})$	1.71	Times, $\tau_k (\text{s})$	0.00	0.30	0.60	0.90	1.20	$T (\text{s})$	3.49
		$\Delta\tau = 0.35 \text{ s}$ and $t_a = 1.75 \text{ s}$													
Amplitudes, $A_k (\text{m/s}^2)$	0.1531	0.1904	0.1760	0.1954	0.1421	$\Psi (\text{mm})$	0.97	Times, $\tau_k (\text{s})$	0.00	0.35	0.70	1.05	1.40	$T (\text{s})$	3.74

4.2 Variations of System and Command-Designing Parameters.

For certain jib parameters and container dimensions, the determination of the magnitudes of the equally spaced steps depends on the number of sloshing modes, n , liquid filling ratio, h/W , step size interval, $\Delta\tau$, and the cable length, a .

4.2.1 Variation of Time-Step. For a certain number of sloshing modes, the selection of a time-step, $\Delta\tau$, is constrained by the maximum jib acceleration, a_{\max} , and the total traveled distance, d . As the time-step decreases, the amplitude of input acceleration increases, which may exceed the predefined maximum

acceleration, a_{\max} , and will result in higher sloshing waves. However, increasing the time-step will increase the distance traveled in the acceleration and deceleration stages, which may exceed the predefined total distance, d . Therefore, there is a range of time-steps satisfying the system constraints. A time-step increment of 0.01 s was used in this analysis. The reason of using this value of increment is to represent the sampling time limitations of the actuator's hardware [2]. For a single sloshing mode with $h/W = 0.1$, the smallest time-step is $\Delta\tau = 0.24 \text{ s}$ and the corresponding maneuver time is $T = 3.19 \text{ s}$. The corresponding magnitudes of the multisteps shaped command and the root-mean-

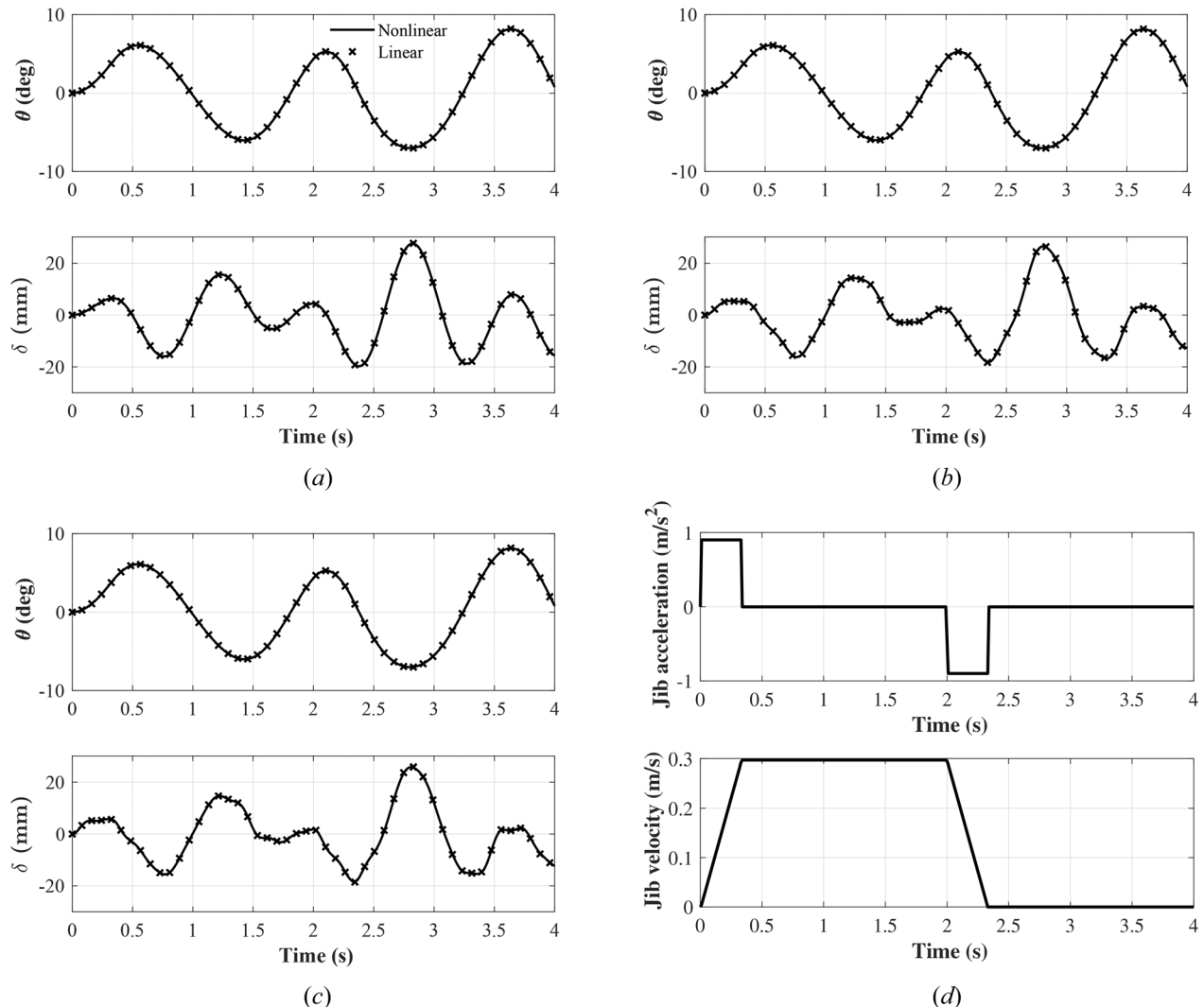


Fig. 2 Dynamic responses of TORB command when using (a) single, (b) three, and (c) five sloshing modes, and (d) TORB command profile ($h/W = 0.1$)

Table 3 Amplitudes of the input steps, the RMS wave surface oscillations, and the total maneuver time for different liquid filling ratios, h/W , and single sloshing mode

$h/W = 0.1, \Delta\tau = 0.24 \text{ s and } t_a = 1.2 \text{ s}$							
Amplitudes, $A_k (\text{m/s}^2)$	0.6544	-0.4807	0.8958	-0.4412	0.6218	$\Psi (\text{mm})$	3.53
Times, $\tau_k (\text{s})$	0.00	0.24	0.48	0.72	0.96	$T (\text{s})$	3.19
$h/W = 0.2, \Delta\tau = 0.21 \text{ s and } t_a = 1.05 \text{ s}$							
Amplitudes, $A_k (\text{m/s}^2)$	0.7512	-0.0857	0.0777	-0.0172	0.7027	$\Psi (\text{mm})$	1.29
Times, $\tau_k (\text{s})$	0.00	0.21	0.42	0.63	0.84	$T (\text{s})$	3.04
$h/W = 0.6, \Delta\tau = 0.20 \text{ s and } t_a = 1.0 \text{ s}$							
Amplitudes, $A_k (\text{m/s}^2)$	0.7846	0.1289	-0.3493	0.1993	0.7365	$\Psi (\text{mm})$	0.23
Times, $\tau_k (\text{s})$	0.00	0.20	0.40	0.60	0.80	$T (\text{s})$	2.99
$h/W = 0.8, \Delta\tau = 0.20 \text{ s and } t_a = 1.0 \text{ s}$							
Amplitudes, $A_k (\text{m/s}^2)$	0.7782	0.0937	-0.2642	0.1587	0.7335	$\Psi (\text{mm})$	0.25
Times, $\tau_k (\text{s})$	0.00	0.20	0.40	0.60	0.80	$T (\text{s})$	2.99

square (RMS) of the wave surface oscillations, Ψ , for three time-steps $\Delta\tau = 0.24, 0.30$, and 0.35 s are listed in Table 2. The dynamics response using the nonlinear form of the governing Eq. (3) and the command acceleration and velocity profiles are illustrated in Fig. 3. From Table 2, increasing the time-steps from 0.24 to 0.30 s increases the maneuver time, T , from 3.19 to 3.49 s (9.4%) and results in reduction of the wave oscillations, Ψ , from 3.53 to 1.71 mm (52%).

4.2.2 Variation of Liquid Depth. The sloshing frequencies of the inside liquid depend on the liquid-filling level to the width of the container, h/W , according to Eq. (A1e) in Appendix A. For a single sloshing mode and the smallest time step-size , the corresponding magnitudes of the multisteps shaped command, the RMS of the wave surface oscillations, and the total traveled time for $h/W=0.1, 0.2, 0.6$, and 0.8 are listed in Table 3. Figure 4 shows the variation of the swing angle, the liquid free-surface

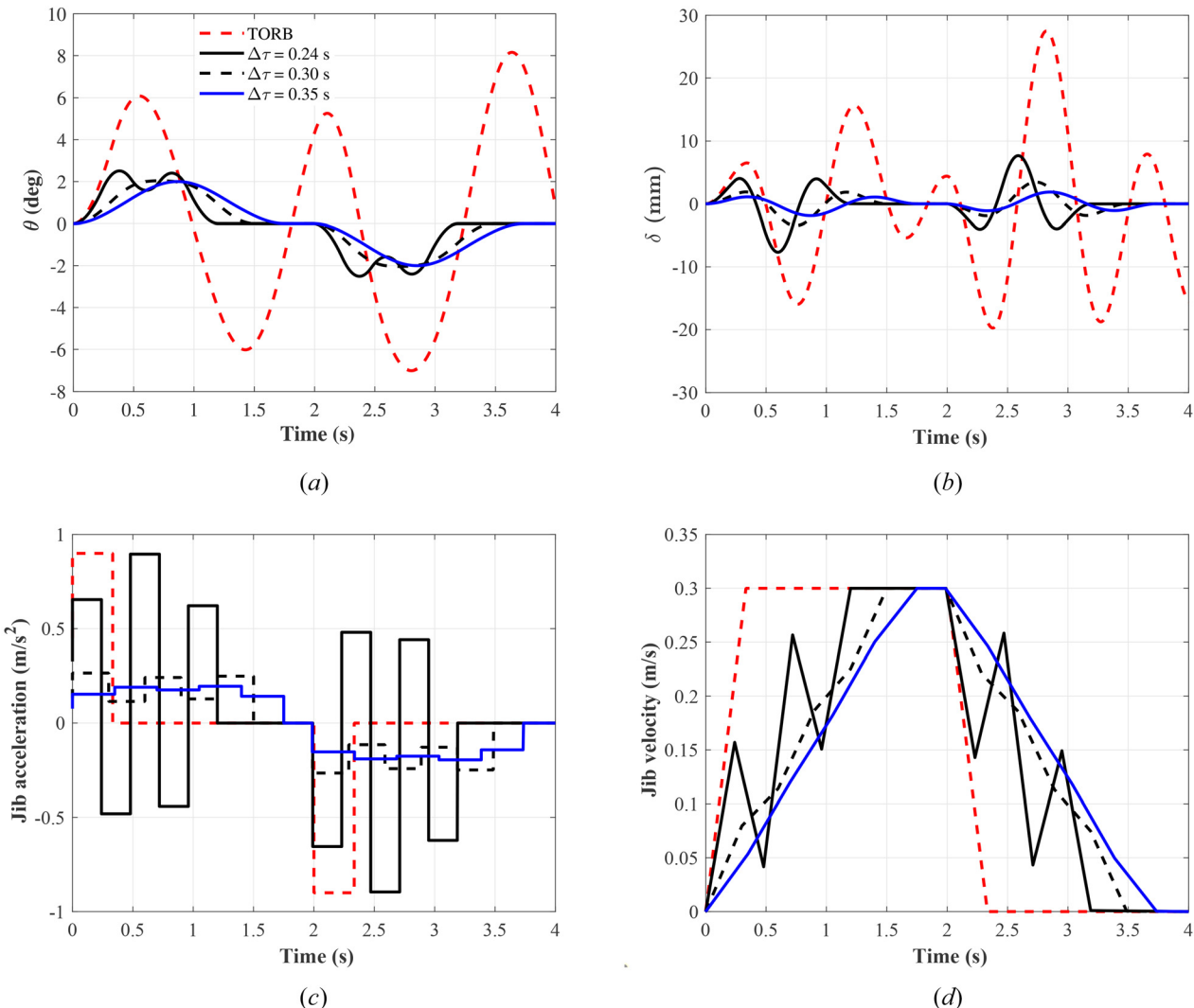


Fig. 3 Dynamic responses of different input-command profiles designed based on different time-steps, $\Delta\tau$ and single sloshing mode ($h/W = 0.1$): (a) swing angle, (b) free-surface wave motion, (c) jib acceleration, and (d) jib velocity

motion, and the acceleration and velocity profiles of the shaped commands. The increase of the liquid depth increases the maximum swing angle and significantly reduces the liquid surface wave motion. The dynamics response and input command profile of $h/W = 0.6$ and 0.8 are almost identical since the sloshing frequencies do not significantly change after the liquid depth reaches a certain critical value. Therefore, it is necessary to employ controlling techniques in conveying a container with shallow liquid depth, $h/W \leq 0.2$.

4.2.3 Variation of Cable Length. The changing of the cable length, a , that attaches the container to the moving jib will mostly alter the swing frequency corresponding to the angular motion, θ . The increasing in the cable length will slightly increase the minimum allowable maneuver time required to satisfy the system constraints. Even though the amplitudes of the input steps were adjusted, the trend of the dynamic response is similar to the one shown in Fig. 3.

4.2.4 Employing Higher Sloshing Modes. The simplicity of designing an input command with a single sloshing mode comes with the cost of increased sensitivity to modeling errors and parameters variations. All the previous analyses were based on modeling the sloshing dynamics using single sloshing mode, $n=1$. Using a liquid depth ratio of $h/W = 0.1$, the dynamic

response and input command profile when employing higher sloshing modes in command designing are illustrated in Fig. 5. Adding sloshing modes in command designing increases the number of steps in the shaped command and results in a higher maneuver time. The free-surface motion of the liquid, δ , is sensitive to how many sloshing modes are used in designing, where in contrast there is no noticeable change in the swing angle, θ . The total maneuver time for a single, three, five, and seven sloshing modes are 3.19, 3.15, 3.28, 3.34 s, respectively. Using three to five sloshing modes are quite sufficient in representing the sloshing dynamics of the inside liquid. Suppressing residual vibrations at higher sloshing modes has a minor improvement while rendering a slower response.

4.3 Transient Sloshing Oscillation Versus Maneuver Time.

The variation of the RMS of the wave surface oscillations versus the maneuver time is shown in Fig. 6(a) when five sloshing modes are used in modeling the sloshing dynamics. The downward trends of the wave motion with the maneuver time are steep for a shallow liquid-filled container ($h/W \leq 0.2$) compared to the deep liquid-filled containers. For instance, the smallest maneuver time and its corresponding largest RMS of the wave motion for liquid depth ratio of 0.1 are 3.23 s and 2.58 mm, respectively. In contrast, to ensure that the jib utilizes the full system capabilities, the smallest maneuver time and its corresponding largest RMS of the wave

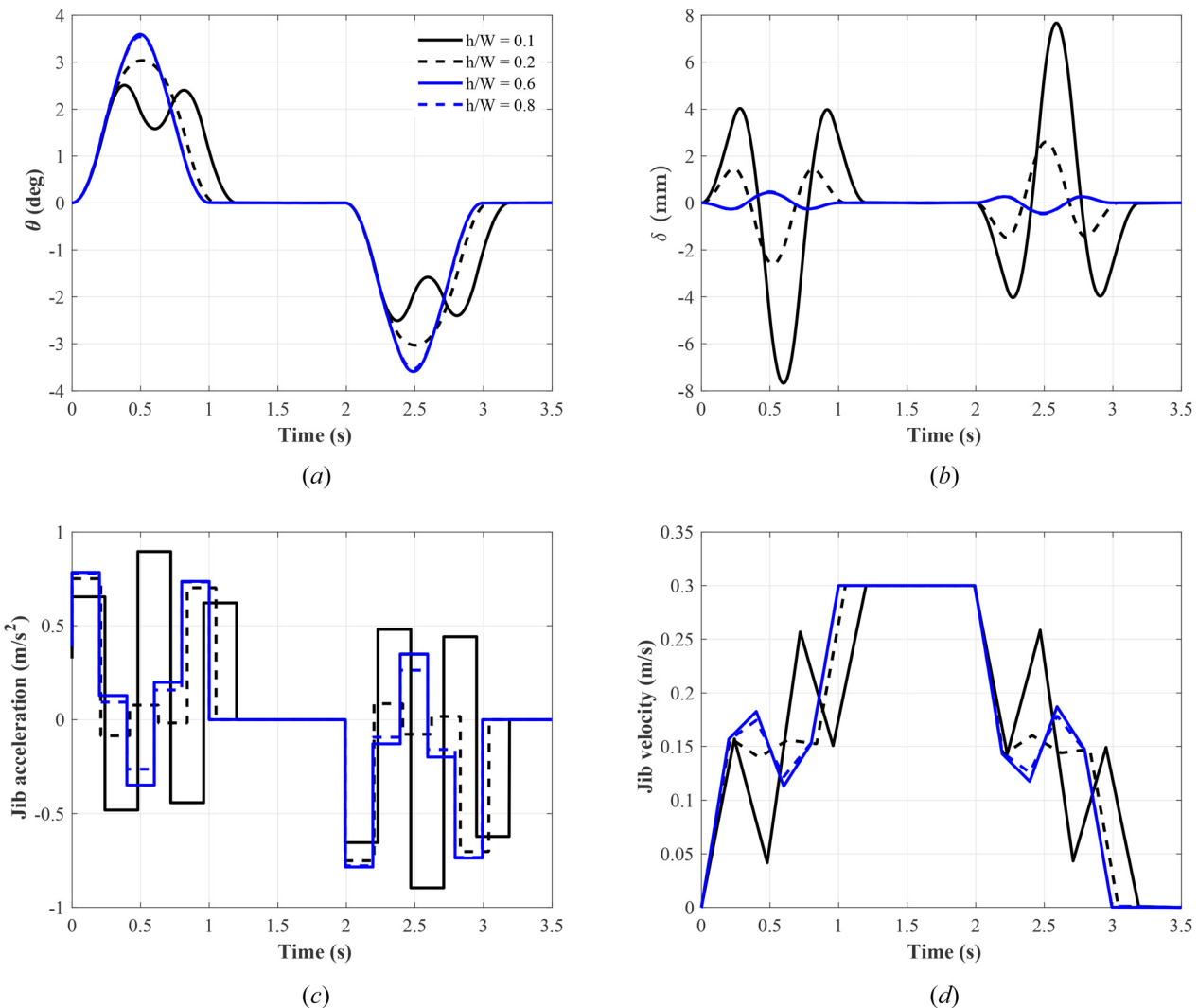


Fig. 4 Dynamic responses of different input-command profiles designed based on different liquid depth ratios, h/W , a single sloshing mode, and the shortest maneuver time: (a) swing angle, (b) free-surface wave motion, (c) jib acceleration, and (d) jib velocity

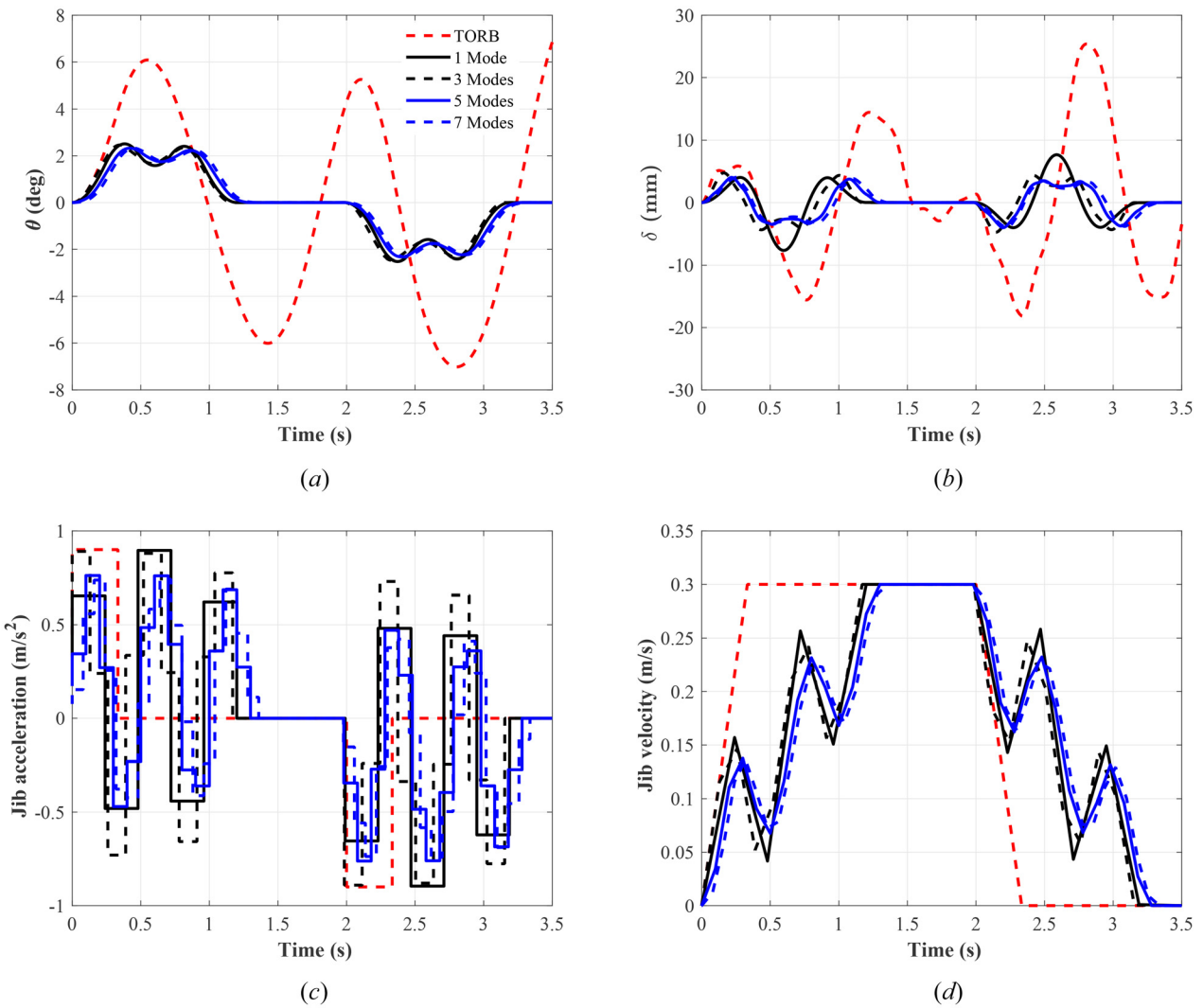


Fig. 5 Dynamic responses of input-command profiles designed based on different sloshing modes, n , and the shortest maneuver time ($h/W = 0.1$): (a) swing angle, (b) free-surface wave motion, (c) jib acceleration, and (d) jib velocity

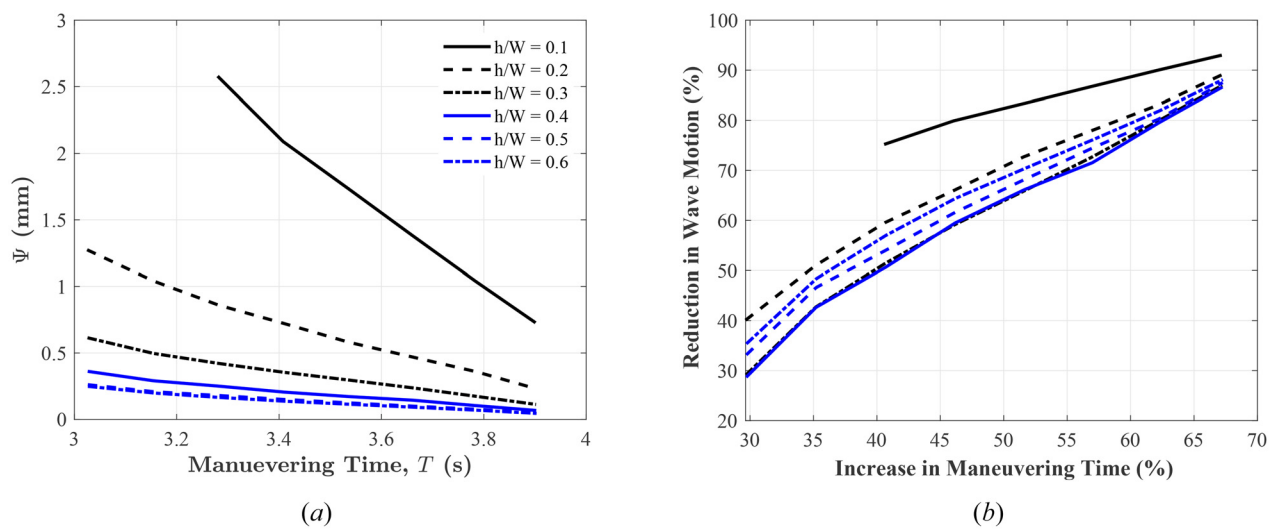


Fig. 6 (a) The variation of the wave surface oscillations versus the maneuver time and (b) the reduction of the wave motion and the increase in maneuver time with respect to TORB command ($n = 5$)

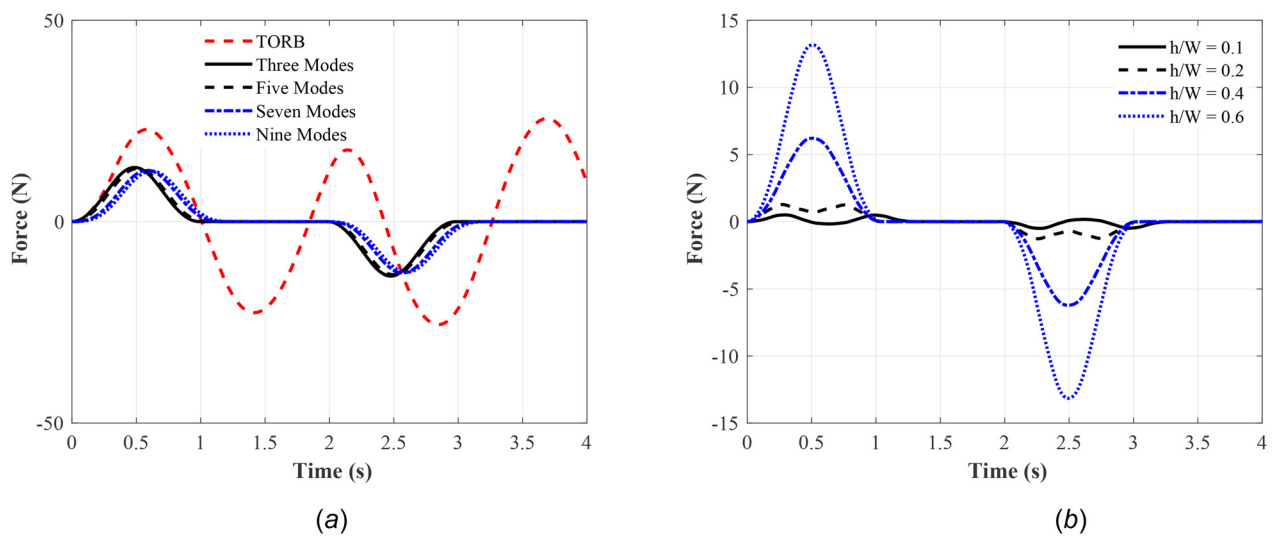


Fig. 7 The exerted force on the container's wall from the water's weight and the induced sloshing force: (a) different sloshing modes; $h/W = 0.6$ and (b) different water depths; $n = 5$

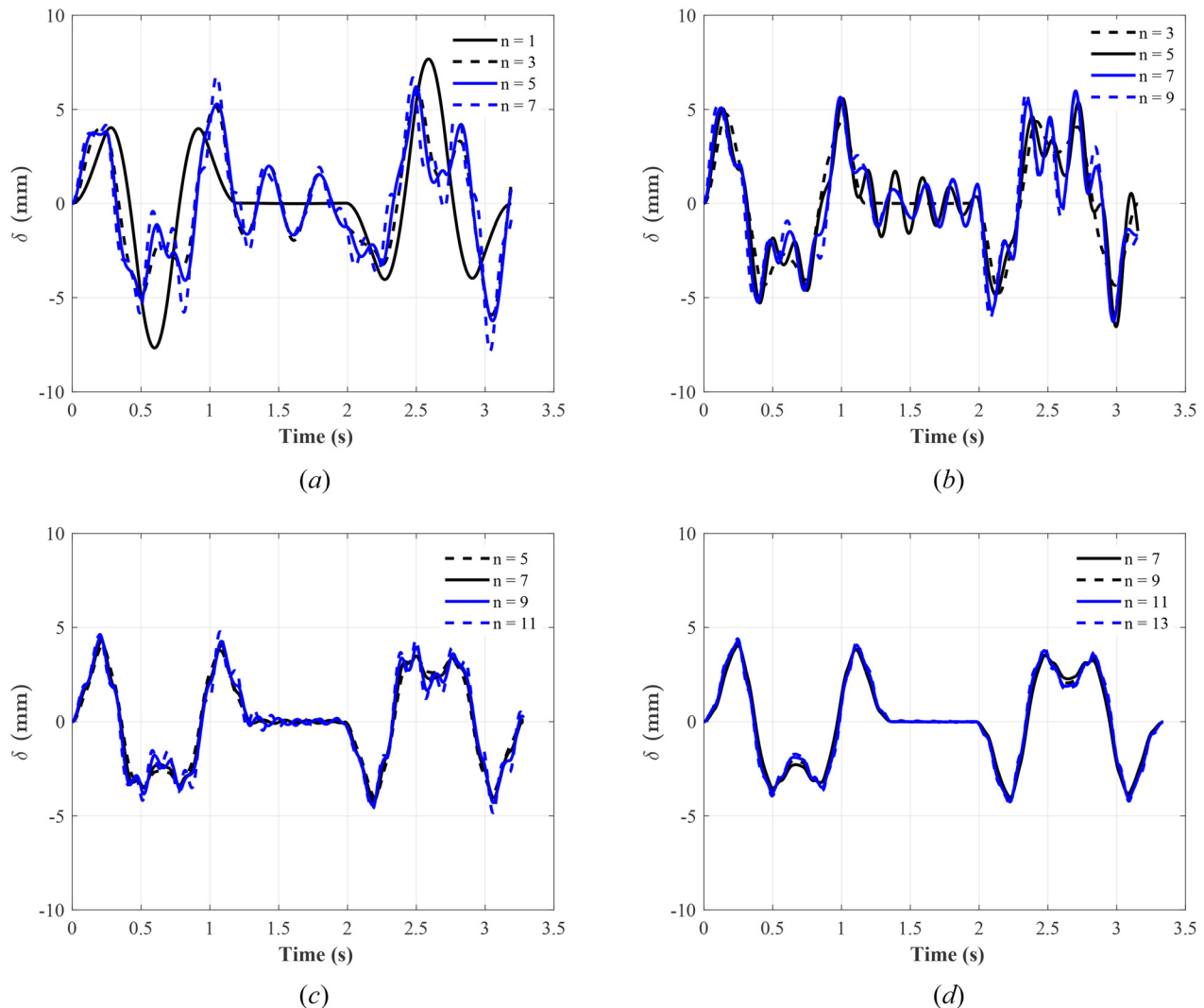


Fig. 8 The free-surface wave motion of higher sloshing modes with input command designed based on (a) 5, (b) 9, (c) 13, and (d) 17 steps ($h/W = 0.1$)

motion for liquid depth ratio of 0.1 are 3.90 s and 0.73 mm, respectively. Therefore, increasing the operational time 21% (3.23 s versus 3.90 s) results of 72% (2.58 versus 0.73 mm) reduction in the induced transient sloshing. However, the reductions of the wave motion in a deep liquid-filled container are insignificant. Figure 6(b) illustrates the reduction of the wave motion versus the increase in the maneuver time compared to the TORB command. Employing command shaping reduces the induced sloshing from 30 to 40% while making the system 30% slower than the TORB for liquid depth ratios from 0.2 to 0.6. For a liquid depth ratio of 0.1, the shaped command reduces sloshing 75% while rendering the response 40% slower than the TORB.

4.4 Structural Fatigue. The total forces exerted into one of the walls from the water's weight and the induced sloshing forces can be computed using Newton's second law as

$$F_x(t) = W_f \sin \theta + \frac{1}{2} \sum_{i=1}^n k_i q_i + c_i \dot{q}_i \quad (11)$$

Figure 7 shows the time response of the exerted force on one of the container's wall. The negative force can be interpreted as the force is now applied to the other container's wall. It is clear from

the response that the forces are fluctuating, i.e., time-varying loading, and hence it will induce structural fatigue. The shaped command reduces the transient force, and hence decreases the induced midrange and alternating forces. Furthermore, the force-free region reduces the number of induced cycles, and hence increases the cycle life of the container. Even though the force magnitude seems to be relatively small for the case of the prototype crane with small dimensions and input parameters, the force magnitude will be higher for an actual crane operating in a real-life application.

4.5 Higher Modes. Since the inside liquid is basically a continuous system that can be modeled by a sufficient n multidegree-of-freedom systems, the input command can be designed using a large number of lumped masses. Naturally, the larger the number of lumped masses used in the equivalent mechanical model, the higher the accuracy of the resulting sloshing analysis. To further assess the effect of sloshing modes in designing a command, the influence of the higher modes in a command designed using lower modes is illustrated in Fig. 8. Figure 8(a) shows the response of higher sloshing modes, $n = 3, 5$, and 7 subjected to a command that was designed using only a single mode, $n = 1$ (five steps). Figures 8(b)–8(d) show the response of higher sloshing modes when subjected to an input predesigned for a lower mode. It is worth noting that the command designed based on seven sloshing

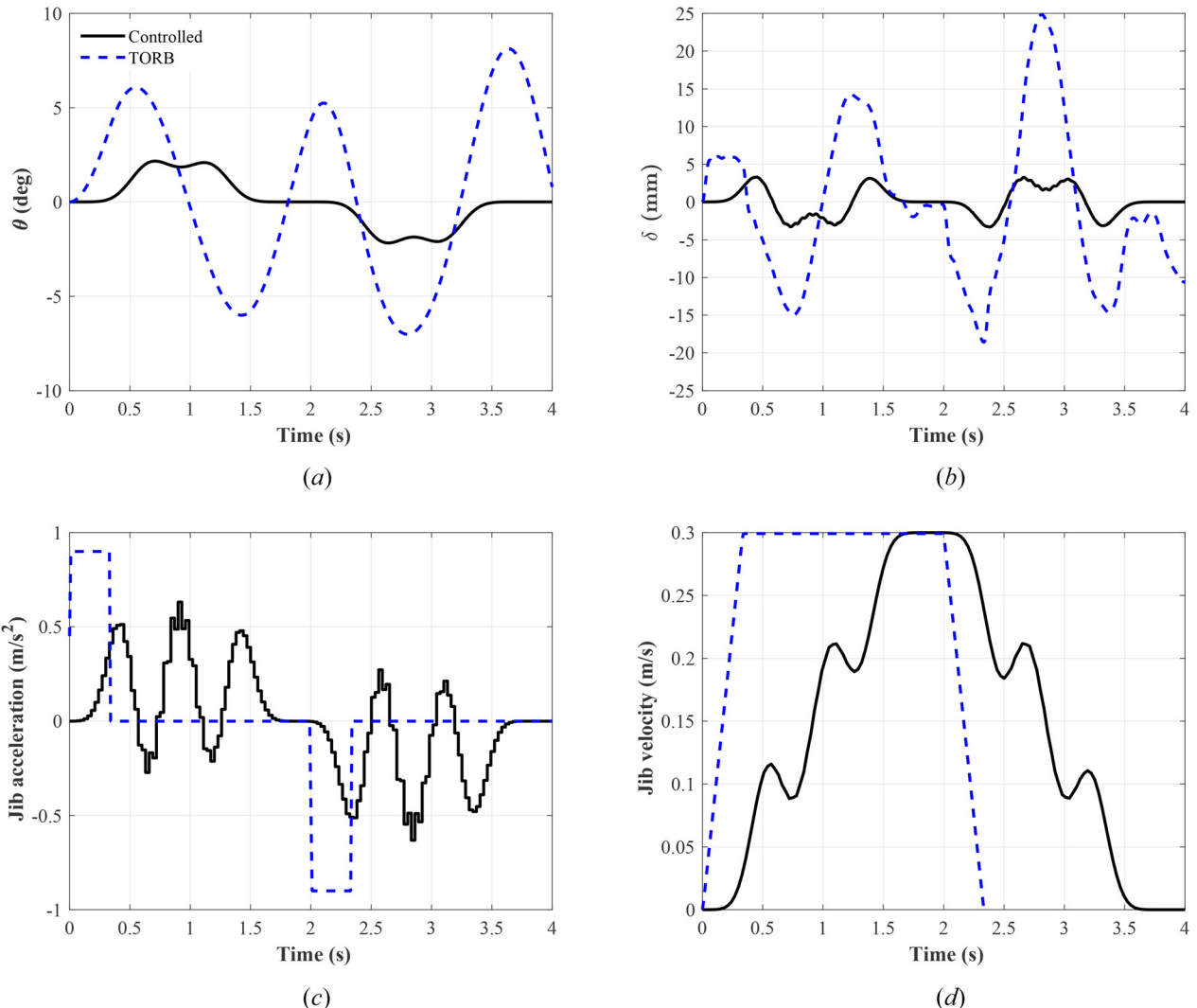


Fig. 9 Dynamic responses of input-command profile designed based on $n = 30$ sloshing modes ($h/W = 0.1$): (a) swing angle, (b) free-surface wave motion, (c) jib acceleration, and (d) jib velocity

Table 4 Amplitudes, forcing frequencies, and phase angles of the smooth sine waves command given in Eq. (12)

$k =$	1	2	3	4	5	6
Amplitudes, A_k (m/s ²)	0.277	0.167	0.253	0.106	0.0414	0.02535
Forcing frequency, Ω_k (rad/s)	0.948	7.685	5.946	1.804	2.491	11.17
Phase angle, ϕ_k (rad)	1.476	2.045	1.861	-2.106	-0.154	-1.012

modes guarantees the elimination of the residual vibrations from the higher modes. However, using five sloshing modes is quite sufficient in reducing the residual vibration from the unmodeled modes.

The input command becomes smoother with the increasing of the employed steps, i.e., retaining higher sloshing modes in command designing. Figure 9 illustrates the dynamics response and command profile when $n=30$ sloshing modes and $\Delta\tau=0.03$ s were used for a liquid depth ratio of $h/W=0.1$. The variations of swing angle and free-surface wave motion are quite similar with those using lower modes, Fig. 5. However, the command profiles, velocity and acceleration, are much smoother, Figs. 9(c) and 9(d).

The shape of the command profile in Fig. 9(c) suggests using a sine wave command. Using the following general sine wave input command:

$$\ddot{u}(t) = \sum_{k=1}^m A_k \sin(\Omega_k t + \phi_k) \quad (12)$$

where A_k , Ω_k , and ϕ_k are fitting parameters that should be determined in a linear-square sense. For $n=30$ sloshing modes, there are $m=63$ steps in Fig. 9(c) that can be used to determine the fitting parameters. Using these magnitudes of the 63 steps, 18 fitting parameters ($m=6$ in Eq. (12)) were determined and listed in Table 4. The dynamics response of the suspended liquid container for a sine waves input of Eq. (12) and the parameters listed in Table 3 are shown in Fig. 10. The responses from the steps and sine waves are almost identical. Even though the fitting parameters were based on the steps magnitudes and not on the system constraints, the response of the sine waves produces zero residual

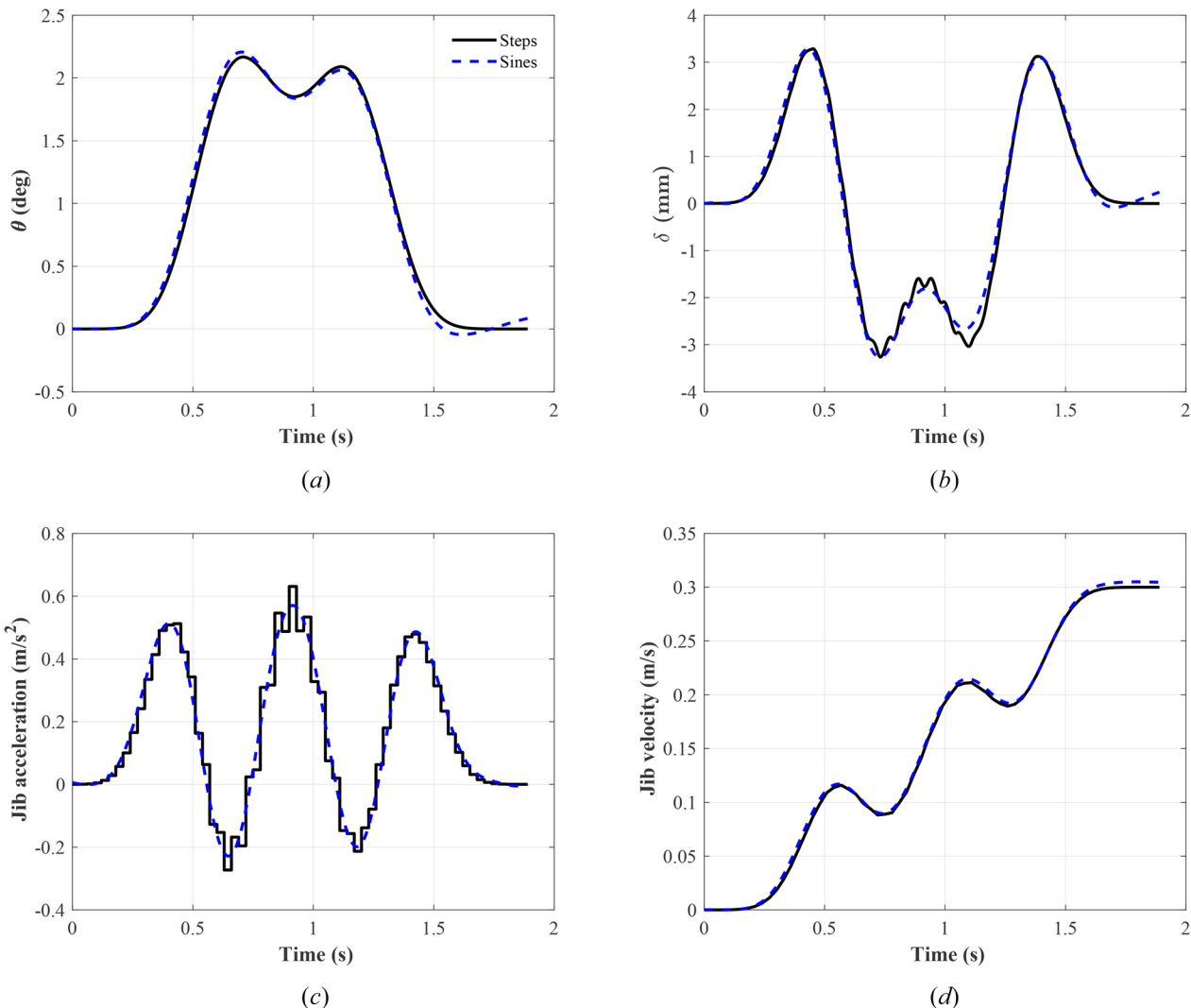


Fig. 10 The comparison between 63 steps and six sine waves command on the dynamics responses ($h/W=0.1$): (a) swing angle, (b) free-surface wave motion, (c) jib acceleration, and (d) jib velocity

vibrations at the end of the acceleration stage. Furthermore, the jib velocity of the sine wave command reaches the maximum jib velocity at the end of the acceleration stage.

4.6 Comparison With Other Input Shaping Techniques.

The proposed multisteps input command is compared with the zero vibration shapers for a multimode system (ZVMM) and the time-optimal flexible-body control (TO ZV), which is characterized by utilizing the full acceleration capability of the actuator and rapid switching of the command between its maximum and minimum acceleration values [18].

4.6.1 Multimode Zero Vibration Shapers. The zero vibration (ZV) shaper for a single mode system is based on convolving a sequence of impulses with system input to generate an output with zero residual vibration [14,17]. If these impulses are designed for each of the vibrational modes independently, they can be convolved to form a sequence, which moves a multimode system without residual vibration. The convolving of multiple mode sequences creates packed impulses that are difficult to implement in real-time, increases the time required to modify the input, and therefore, decreases in servovate performance [15]. Hence, the multiple mode sequences can be alternatively generated by direct solution of the following constraint equations:

$$\sum_{k=1}^m A_k e^{\zeta_j \omega_j t_k} \sin\left(\omega_j \sqrt{1 - \zeta_j^2} t_k\right) = 0, \quad \text{for } j = 1, 2, \dots, N \quad (13a)$$

$$\sum_{k=1}^m A_k e^{\zeta_j \omega_j t_k} \cos\left(\omega_j \sqrt{1 - \zeta_j^2} t_k\right) = 0, \quad \text{for } j = 1, 2, \dots, N \quad (13b)$$

$$\sum_{k=1}^m A_k = a_{\max} \quad (13c)$$

where A_k is the impulse amplitude and t_k is the time at which the impulse occurs, $m = N + 1$ is the number of required impulses, and N is the number of modes in the vibrational system. The two first equations guarantee the elimination of the residual vibrations where the last equation ensures that the none of the generated impulses exceeds the input limitation, e.g., maximum acceleration. It is clear that there are $2m = 2N + 2$ unknowns of A_k and t_k in $2N + 1$ equations; therefore, t_1 can be set to zero (origin specification). The nonlinear equations were solved using the numerical optimization fmincon in MATLAB to find the magnitudes and times of the impulses that minimizes (not theoretically eliminates) the residual vibrations with the shortest maneuver time.

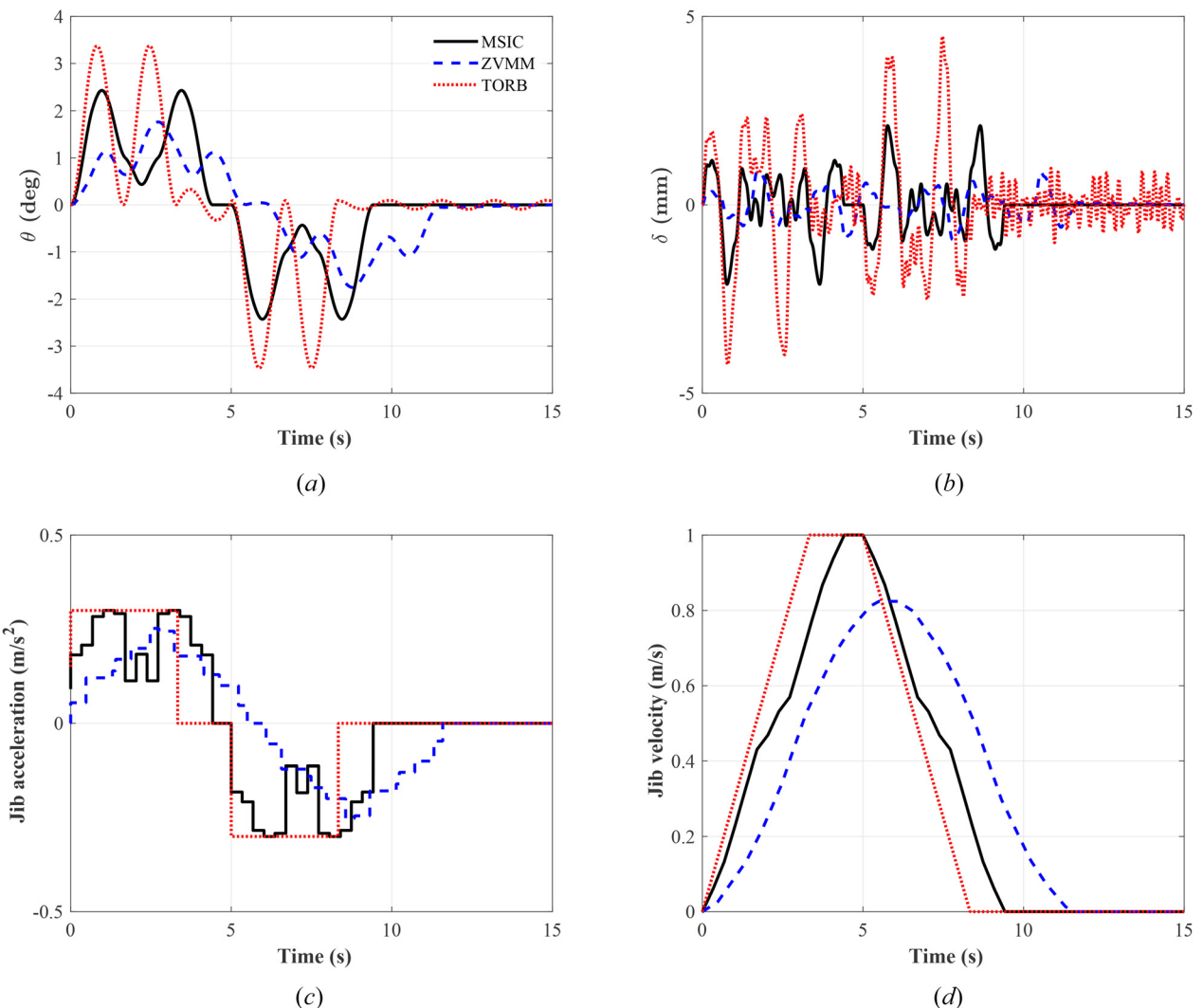


Fig. 11 Comparison between the MSIC and ZVMM with their corresponding dynamic responses ($h/W = 0.1$ and $n = 5$): (a) swing angle, (b) free-surface wave motion, (c) jib acceleration, and (d) jib velocity

Figure 11 shows the responses of the suspended system with water depth ratio of $h/W = 0.1$ and negligible damping (worst-case scenario) when employing the proposed MSIC and ZVMM. The jib kinematics for this comparison are $a_{\max} = 0.3 \text{ m/s}^2$, $v_f = 1 \text{ m/s}$, and $d = 5 \text{ m}$. It is clear from Figs. 11(c) and 11(d) that the ZVMM does not utilize the full actuator capability. For this reason, the transient vibration amplitudes of ZVMM are less than the induced amplitudes from MSIC.

4.6.2 Time-Optimal Flexible-Body Control. The command profile of a time-optimal flexible-body control can be written in the form of Eq. (6) as

$$\ddot{u}(t) = a_{\max} H_{\tau_1} + 2a_{\max} \sum_{i=2}^m (-1)^{i-1} H_{\tau_i} \quad (14)$$

where the time locations τ_i are determined by imposing the conditions of Eq. (9). Due to the transcendental nature of these constraints, the equations may have none, one, or many solutions that satisfying the constraint equations while ensuring the jib velocity and the traveled distance are not exceeding the predefined values v_f and d , respectively. The desired time-optimal command was found using numerical optimization. Figure 12 shows a comparison between the time-optimal flexible-body control (denoted as

TO ZV) and the multisteps input command (denoted as MSIC). Even though the TO ZV has a relatively smaller maneuver time compared to the MSIC, the TO ZV does not guarantee the elimination of the residual vibrations from the higher modes, Figs. 12(a) and 12(b).

Furthermore, the optimal time locations τ_i of the ZVMM and TO ZV may not be within the sampling time of the actuator's hardware. The transient oscillations are greater for the TO ZV. It is worth noting that it was easy to implement and designed the shaped MSIC, which is based on a system of simultaneous linear equations, Eq. (10), than designing ZVMM or TO ZV that requires optimization and results of time optimal locations that could not be practically implemented. Given the numerous advantages provided by the proposed MSIC in suppressing the residual sloshing, it provides an attractive alternative to the ZVMM and TO ZV commands.

4.7 Sensitivity Analysis. For completeness, a parametric sensitivity analysis is conducted by designing a command input profile assuming certain values of the system parameters and then applying it to models with different parameter values. The sloshing frequencies of the suspended system are changing during motion due to the changes of the liquid depth. The robustness test based on observing the residual vibrations at different liquid

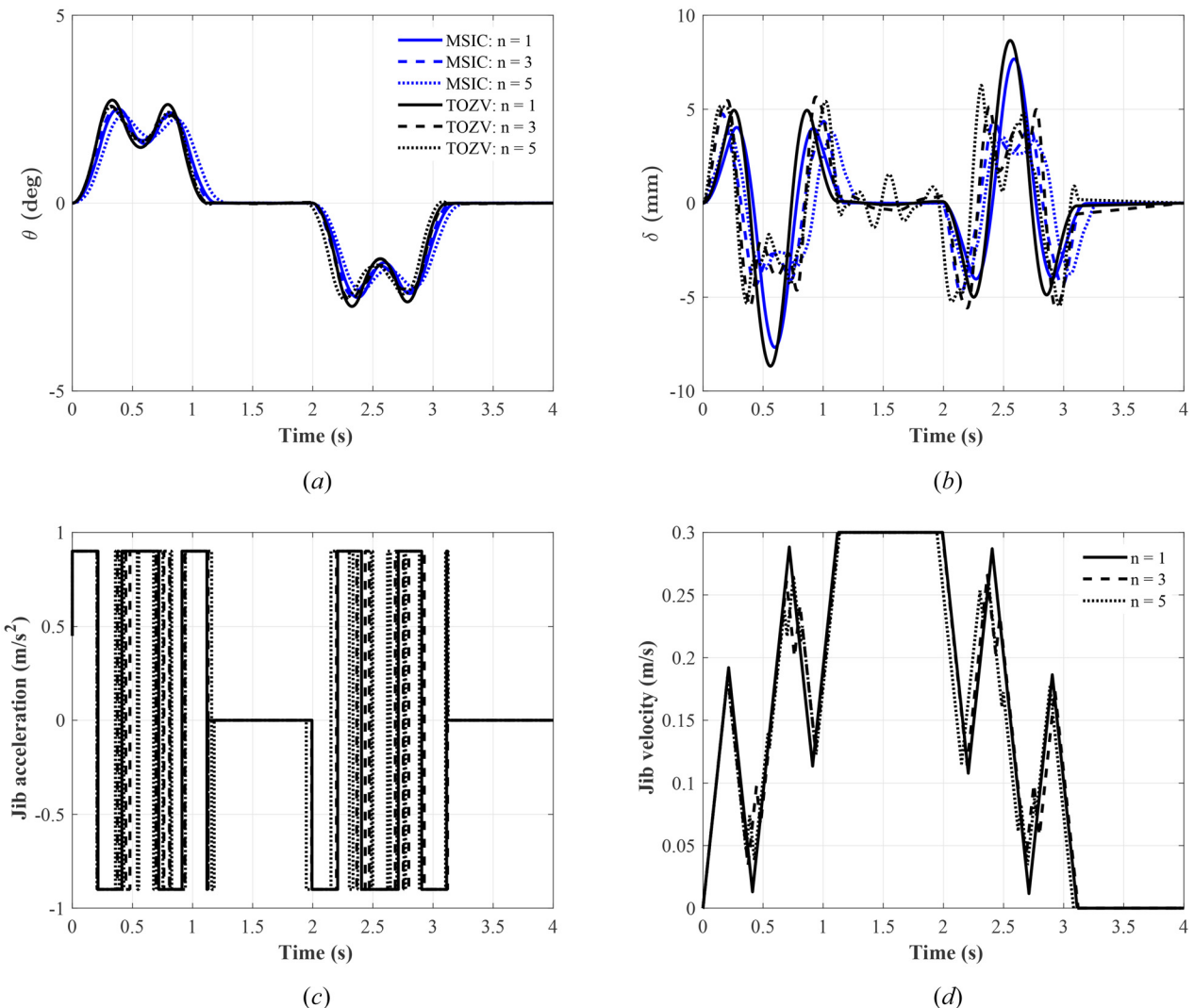
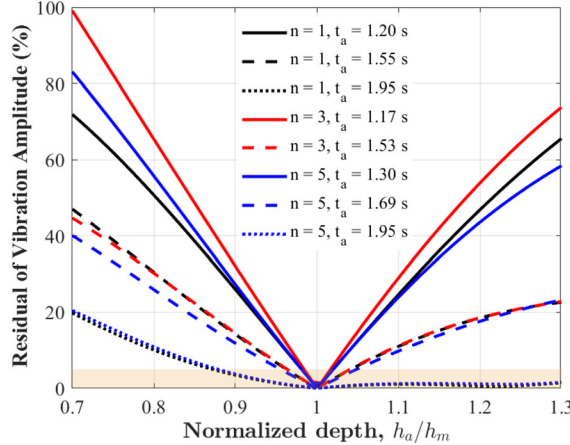


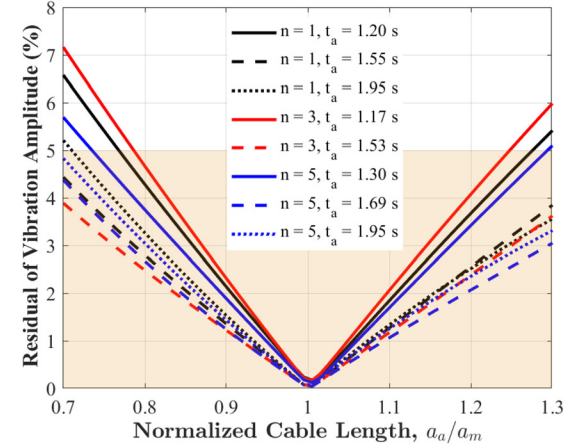
Fig. 12 Comparison between the MSIC and TO ZV with their corresponding dynamic responses using different values of the sloshing modes ($h/W = 0.1$): (a) swing angle, (b) free-surface wave motion, (c) jib acceleration, and (d) jib velocity

depths while fixing the input command represents a practical scenario that captures the command performance with the varying liquid depth during the maneuver. The vibration amplitude at the end of the command interval (acceleration stage) is computed as

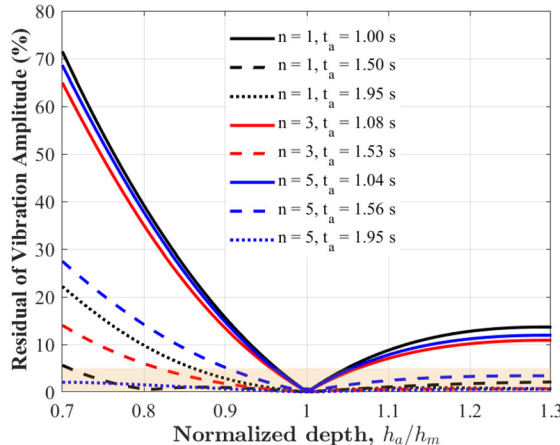
$$\text{Vib. Amp.} = \sqrt{\theta(t_a)^2 + \left(\frac{\dot{\theta}(t_a)}{\omega_{n,1}}\right)^2} + \frac{1}{h} \sum_{i=1}^n \sqrt{q_i(t_a)^2 + \left(\frac{\dot{q}_i(t_a)}{\omega_{n,i+1}}\right)^2} \quad (15)$$



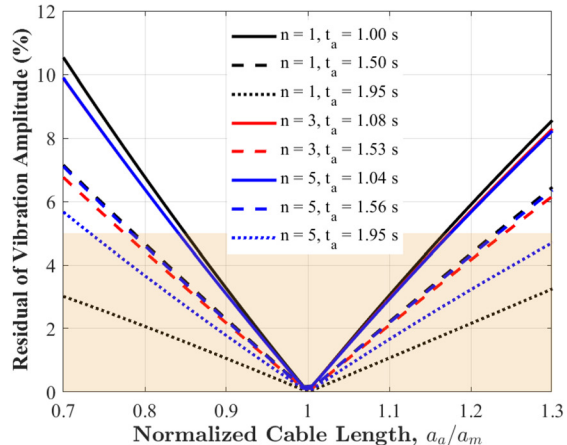
(a)



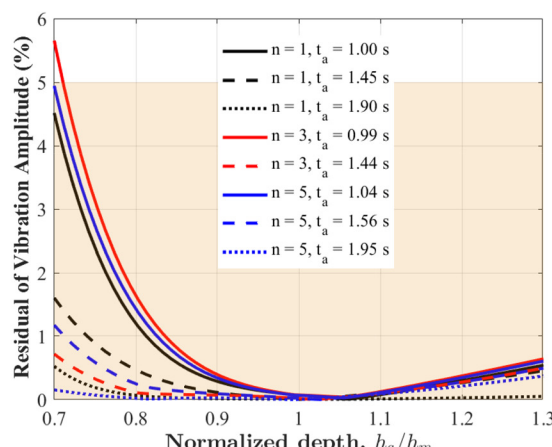
(b)



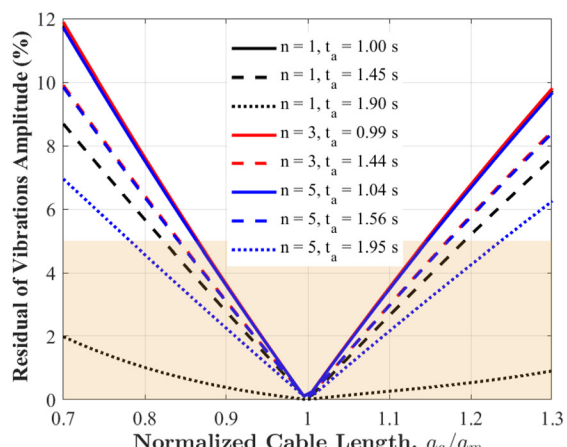
(c)



(d)



(e)



(f)

Fig. 13 Sensitivity analysis of the proposed input commands to the changes of liquid depth and cable length for different sloshing modes, n , and command interval, t_a : (a) $h_m = 25 \text{ mm}$ ($h/W = 0.1$) and $a = 0.3 \text{ m}$, (b) $h = 25 \text{ mm}$ ($h/W = 0.1$) and $a_m = 0.3 \text{ m}$, (c) $h_m = 50 \text{ mm}$ ($h/W = 0.2$) and $a = 0.3 \text{ m}$, (d) $h = 50 \text{ mm}$ ($h/W = 0.2$) and $a_m = 0.3 \text{ m}$, (e) $h_m = 100 \text{ mm}$ ($h/W = 0.4$) and $a = 0.3 \text{ m}$, and (f) $h = 100 \text{ mm}$ ($h/W = 0.4$) and $a_m = 0.3 \text{ m}$

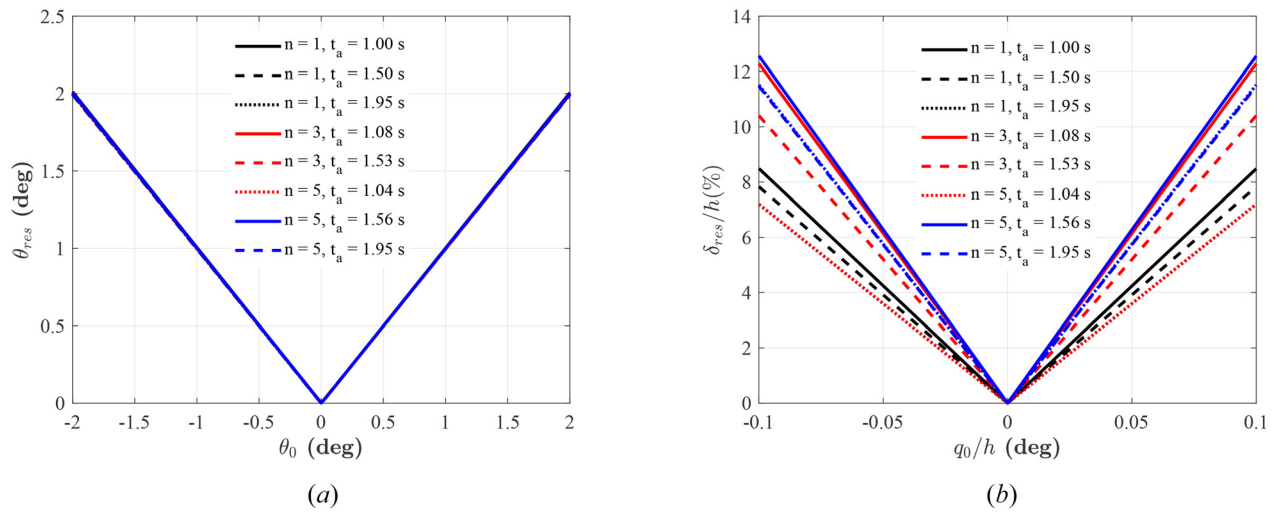


Fig. 14 Residual vibration amplitude when the system subjected to an initial disturbance in the form of (a) θ_0 and (b) q_{10} while using different sloshing modes and different command intervals ($h/W = 0.2$)

where $\omega_{n,i}$ is the system natural frequencies obtained from the characteristic polynomial Eq. (B3). The percentages of the residual vibrations which is the amount of residual vibration amplitudes when using the shaped command divided by the amplitudes of residual vibrations when using TORB versus the changes of the cable length and liquid depth are illustrated in Fig. 13. The robustness is measured quantitatively by measuring the width of the sensitivity curve at some low vibration level (shaded area represents 5% vibration tolerance).

For instance, using a shaped command designed based on a cable length of 0.3 m and a modeled depth of $h_m = 25$ mm ($h/W = 0.1$), the percentage of the numerically simulated residual vibration amplitude when the liquid depth varies $\pm 30\%$ from its modeled depth, i.e., $0.7 \leq h_a/h_m \leq 1.3$ is plotted in Fig. 13(a) for different sloshing modes and command intervals. The command becomes less sensitive to the changes of liquid depth with the increasing in the command interval. The robustness of the shaped command with a command interval of 1.95 s is $h_a/h_m > 0.88$. The sensitivity when using different sloshing modes becomes coincident with each other with the increasing in the command interval. The robustness is increased for deep liquid depths, Figs. 13(c) and 13(e). A designed input command is expected to give inferior performance when the modeled depth, h_m , is smaller than the actual operating depth, h_a .

The sensitivity analysis of the input commands to the changes in cable length was also conducted. Using a shaped command designed based on a cable length of $a_m = 0.3$ m and different water depths $h = 25$ mm ($h/W = 0.1$), 50 mm ($h/W = 0.3$), and 100 mm ($h/W = 0.4$), the percentages of the numerically simulated residual vibration amplitude when the cable length varies $\pm 30\%$ from its modeled length, i.e., $0.7 \leq a_a/a_m \leq 1.3$ are plotted in Figs. 13(b), 13(d), and 13(f) for different sloshing modes and command intervals. The shaped command is more sensitive to the changes of cable length for a shallow liquid depth ($h/W = 0.1$) compared to the deep liquid depths ($h/W \geq 0.2$). The sensitivity curves for different liquid depths are similar since changing the cable length will mainly alter the swinging frequency.

4.8 Initial Disturbance. All the previous analyses were based on assuming zero initial states. Therefore, to assess the effect of the initial disturbances in the command performance, the shaped commands designed based on zero initial conditions are used to command a system with initial disturbances. The residuals

of the numerically simulated vibration amplitudes when the system was disturbed by either an initial swing angle, $-2 \text{ deg} \leq \theta_0 \leq 2 \text{ deg}$ or liquid motion amplitude, q_{10} , within 10% of its nominal depth, are plotted in Fig. 14. The initial disturbance does not affect the command performance in eliminating the residual vibration as illustrated in Fig. 14. It is clear that the shaped command at the end of the acceleration stage will neither eliminate the initial disturbance nor induce any additional residual vibration. This analysis represents a practical scenario when a shaped input profile is used in commanding a system which is not completely stationary. This supports the stability of the shaped command that its performance in eliminating the vibration residuals is not degraded with the existence of initial system disturbances.

5 Conclusions

A dynamical model for an overhead crane conveying a suspended liquid container with multiple sloshing modes has been presented. The response due to the sloshing modes is highly dependent on the ability of keeping the container free from vibrations. A shaped command that consisted of a series of steps was designed to target the system's dynamical behavior and eliminate the residual sloshing to achieve rest-to-rest maneuver. Even though the input command slows down the system and increases the total traveled time, the reduction of the liquid transient and residual oscillations during the overall motion is significant. Suppressing unwanted oscillations at higher sloshing modes has a minor improvement while rendering a slower response. The effectiveness of the proposed input command was demonstrated using numerical simulation. The proposed command considers the effect of liquid damping, utilizes the full capabilities of the system input (unlike traditional zero vibration shaper), and provides adjustable command length (unlike time-optimal flexible-body control) that can be selected based on the actuator's sampling time. The robustness of the proposed input command to suppress sloshing over a range of liquid depths and cable lengths was tested using sensitivity analyses. These analyses suggest to underestimate the liquid depth when designing an input command. Command shaping is sensitive to the changes in the liquid depth for a shallow liquid depth, $h/W \leq 0.2$. In addition to eliminating the residual sloshing, the increasing of the adjustable command length decreases the transient sloshing amplitude and enhances the robustness of the shaped command. Lowering the transient sloshing reduces operational risks when conveying hazardous liquids, while eliminating

residual sloshing renders efficient and accurate operations and reduces the maneuver time.

Unlike the previous works in Refs. [5], [6], and [8] where input shapers are designed based on the natural frequencies obtained from Graham's model, the proposed command considers the effect of swing motion on the sloshing frequency. The proposed multisteps input command was capable of eliminating the residual vibration amplitudes regardless of the number of modes. Several remarks should be considered when designing an input command for suppressing sloshing in moving containers: (a) the necessity of employing controlling techniques in a shallow liquid depth, $h/W \leq 0.2$, (b) at least three sloshing modes should be used when modeling the sloshing dynamics, (c) the command duration, $\Delta\tau$, should be selected to compensate between the operational speed, robustness, and the desired transient reduction in the wave motion, and (d) the fluid depth should be understated in command designing.

The problem of the input command sensitivity can be tackled by adding extra constraints in the command designing such as setting the derivative of the residual vibrations with respect to a certain model parameter, e.g., natural frequency, to zero. It is also possible to use a larger number of steps, more than the minimum number $m = 2n + 3$ that is required to satisfy the rest-to rest maneuvers, where the excess can be used to enhance robustness. Furthermore, one also could impose an additional constraint or select an appropriate command duration that limits the maximum free-surface wave motion to be lower than a certain predefined value. The latter constraint is useful for applications that prevents spillage of hazardous material during motion of partially filled containers. This is also can be achieved by retaining more steps and determining the values of the excess steps by optimizing the maximum wave surface motion. Since the proposed input command was designed based on the linear model; for higher speeds, the nonlinear model should be used in command designing.

Acknowledgment

The authors wish to thank Dima Almujarrab at Kuwait University.

Funding Data

This research received no specific grant from any funding agency in the public, commercial, or not-for-profit sectors.

Nomenclature

- a = length of the rigid link
- $a_j, b_{i,j}, c_j, d_{i,j}$ = complex coefficients of the general solution of θ and q_1
- \mathbf{A} = coefficient matrix
- A, B, C_i, D_i = constants which are functions of initial conditions
- A_i = amplitudes of input shaped command
- \mathbf{c} = vector of input amplitudes,
 $\mathbf{c} = \{A_1 \ A_2 - A_1 \ \cdots \ A_m - A_{m-1}\}^T$
- c_i = equivalent viscous damper constant of the i th sloshing mode
- d = travel distance
- g = gravitational constant, $g = 9.81 \text{ m/s}^2$
- h = liquid filling level
- H = container height
- h_i = distance from liquid center of gravity, $h/2$, to the equivalent i th mass point, m_i
- h_0 = distance from liquid center of gravity, $h/2$, to the liquid rigid mass, m_0
- H_{τ_i} = heaviside function, $H_{\tau_i} = H(t - \tau_i)$
- I_c = mass moment of inertia of the container
- I_{eq} = equivalent mass moment of inertia,
 $I_{eq} = I_c + m_c l_c^2 + I_0 + m_0 l_0^2 + \sum_{i=1}^n m_i l_i^2$
- I_0 = mass moment of inertia of the liquid rigid mass,
 m_0

k_i = equivalent spring stiffness constant of the i th sloshing mode

l_c = distance from jib to container's center of mass,

$$l_c = a + H/2$$

l_i = distance from jib to i th lumped mass, m_i ,

$$l_i = a + H - h/2 - h_i$$

l_0 = distance from jib to liquid fixed-mass, m_0 ,

$$l_0 = a + H - h/2 + h_0$$

m = number of steps in the shaped command

m_c = mass of the container

m_f = total liquid mass, $m_f = \rho Wh = \sum_{i=0}^n m_i$

m_i = equivalent mass of the i th sloshing mode

m_0 = rigid mass of the fixed liquid

n = number of liquid sloshing modes

q_i = lateral displacement of the lumped mass m_i , i.e., surface wave oscillation

\dot{q}_i, \ddot{q}_i = lateral velocity and acceleration of the lumped mass m_i

t = time coordinate

T = total traveled (maneuver) time, $T = t_a + t_c + t_d$

t_a, t_c, t_d = time interval of acceleration, cruising, and deceleration stages, respectively

u, \dot{u}, \ddot{u} = jib horizontal displacement, velocity, and acceleration

W = container width

ζ = liquid damping ratio

η = liquid free-surface elevation

θ = swing angle in xy -plane measured clockwise from vertical y -direction

$\dot{\theta}, \ddot{\theta}$ = angular velocity and angular acceleration

ρ = liquid density

τ_i = time of the amplitudes of input shaped command

ϕ_i = mode shape of the i th sloshing mode

ω_i = natural frequency of the i th sloshing mode

ω_n = natural frequency of the liquid suspended system

(\cdot) = time derivative, d/dt

Appendix A: Equivalent Mechanical Model Parameters

The model parameters of a two-dimensional rectangular rigid-walled container of width W (in the direction of wave motion) and height H with a liquid filling level h are given by [20]

$$m_i = \frac{8m_f}{\pi^3} \frac{\tanh((2i-1)\pi h/W)}{(2i-1)^3 h/W} \quad (\text{A1a})$$

$$\frac{h_i}{h} = \frac{1}{2} - \frac{\tanh((2i-1)\pi h/2W)}{(2i-1)\pi h/2W} \quad (\text{A1b})$$

$$k_i = 8m_f g \frac{\tanh^2((2i-1)\pi h/W)}{\pi^2 (2i-1)^2 h} \quad (\text{A1c})$$

$$c_i = 2\zeta\omega_i m_i \quad (\text{A1d})$$

$$\omega_i = \sqrt{\frac{k_i}{m_i}} = \sqrt{\frac{\pi g}{W} (2i-1) \tanh\left((2i-1) \frac{\pi h}{W}\right)} \quad (\text{A1e})$$

$$m_0 = m_f - \sum_{i=1}^n m_i \quad (\text{A1f})$$

$$h_0 = -\frac{1}{m_0} \sum_{i=1}^n m_i h_i \quad (\text{A1g})$$

$$I_0 = I_F - m_0 h_0^2 - \sum_{i=1}^n m_i h_i^2 \quad (\text{A1h})$$

$$I_F = \frac{m_f}{12} \left[h^2 - 3W^2 + \frac{768W^3}{\pi^5 h} \sum_{i=1}^n \frac{\tanh((2i-1)\pi h/2W)}{(2i-1)^5} \right] \quad (\text{A1i})$$

where m_i , k_i , and c_i ($i = 1, 2, \dots, n$) denote the equivalent mass, equivalent spring stiffness constant, and equivalent viscous damper constant of the i th sloshing mode, respectively; h_i denotes the distance from the liquid center of gravity, $h/2$, to the equivalent i th mass point; m_0 and I_0 denote the rigid mass and mass moment of inertia of the fixed liquid that moves with the container; h_0 is the distance from the liquid center to the rigid mass, m_0 ; $m_f = \rho Wh = \sum_{i=0}^n m_i$ denotes the total liquid mass in the container; ω_i corresponds to the natural frequency of the i th sloshing mode of a liquid surface when the rectangular container is only moved in the lateral direction; ζ is the liquid damping ratio; ρ is the liquid density; and g is the gravitational acceleration.

Appendix B: Constants and Polynomial Expressions in the General Response Solution

The complex coefficients a_j , $b_{i,j}$, c_j , and $d_{i,j}$ for $j = 1, 2, \dots, 2n+2$ in Eqs. (7) and (8) are given by

$$a_j = \frac{A + \sum_{k=1}^n C_k m_k l_k \prod_{k=1}^{2n+1} (\sigma_j - \mu_k)}{I_{\text{eq}} - \sum_{k=1}^n m_k l_k^2 \prod_{\substack{k=1 \\ k \neq j}}^{2n+2} (\sigma_j - \sigma_k)} \quad (\text{B1a})$$

$$b_{i,j} = \frac{Al_i + C_i I_{\text{eq}} + \sum_{k=1}^n m_k l_k (l_i C_k - C_i l_k) \prod_{k=1}^{2n+1} (\sigma_j - \nu_{i,k})}{I_{\text{eq}} - \sum_{k=1}^n m_k l_k^2 \prod_{\substack{k=1 \\ k \neq j}}^{2n+2} (\sigma_j - \sigma_k)}, \quad \text{for } i = 1, 2, \dots, n \quad (\text{B1b})$$

$$c_j = \frac{M_l - \sum_{k=1}^n m_k l_k \prod_{k=1}^{2n} (\sigma_j - \rho_k)}{I_{\text{eq}} - \sum_{k=1}^n m_k l_k^2 \sigma_j \prod_{\substack{k=1 \\ k \neq j}}^{2n+2} (\sigma_j - \sigma_k)} \quad (\text{B1c})$$

$$d_{i,j} = \frac{M_l l_i - I_{\text{eq}} + \sum_{k=1}^n m_k l_k (l_k - l_i) \prod_{k=1}^{2n} (\sigma_j - \kappa_{i,k})}{I_{\text{eq}} - \sum_{k=1}^n m_k l_k^2 \sigma_j \prod_{\substack{k=1 \\ k \neq j}}^{2n+2} (\sigma_j - \sigma_k)}, \quad \text{for } i = 1, 2, \dots, n \quad (\text{B1d})$$

and for $j = 2n+3$

$$c_{2n+3} = \frac{M_l - \sum_{k=1}^n m_k l_k \prod_{k=1}^{2n} \rho_k}{I_{\text{eq}} - \sum_{k=1}^n m_k l_k^2 \prod_{k=1}^{2n+2} \sigma_k} \quad (\text{B2a})$$

$$d_{i,2n+3} = \frac{M_l l_i - I_{\text{eq}} + \sum_{k=1}^n m_k l_k (l_k - l_i) \prod_{k=1}^{2n} \kappa_{i,k}}{I_{\text{eq}} - \sum_{k=1}^n m_k l_k^2 \prod_{k=1}^{2n+2} \sigma_k}, \quad \text{for } i = 1, 2, \dots, n \quad (\text{B2b})$$

The $2n+2$ values of σ_j are the roots of the following characteristic polynomial:

$$\sigma(s) = (I_{\text{eq}} s^2 + M_l g) \prod_{i=1}^n M_i(s) - \sum_{i=1}^n \left[m_i (l_i s^2 + g)^2 \prod_{\substack{j=1 \\ j \neq i}}^n M_j(s) \right] \quad (\text{B3})$$

where $M_i(s) = s^2 + 2\zeta\omega_i s + \omega_i^2$. Similarly, the $2n+1$ values of μ_j and $2n$ values of ρ_j are the roots of the following polynomials:

$$\mu(s) = (As + B) \prod_{i=1}^n M_i(s) + \sum_{i=1}^n \left[m_i (l_i s^2 + g) (C_i s + D_i) \prod_{\substack{j=1 \\ j \neq i}}^n M_j(s) \right] \quad (\text{B4})$$

$$\rho(s) = M_l \prod_{i=1}^n M_i(s) - \sum_{i=1}^n \left[m_i (l_i s^2 + g) \prod_{\substack{j=1 \\ j \neq i}}^n M_j(s) \right] \quad (\text{B5})$$

where the constants A, B, C_i , and D_i are functions of the initial conditions

$$A = I_{\text{eq}} \theta_0 - \sum_{i=1}^n m_i l_i q_{i0}, \quad B = I_{\text{eq}} \dot{\theta}_0 - \sum_{i=1}^n m_i l_i \dot{q}_{i0} \\ C_i = q_{i0} - \theta_0 l_i, \quad D_i = \dot{q}_{i0} - l_i \dot{\theta}_0 + 2\zeta\omega_i q_{i0}, \quad \text{for } i = 1, 2, \dots, n$$

Finally, the $2n+1$ values of $\nu_{i,j}$ and $2n$ values of $\kappa_{i,j}$ for each of the sloshing modes, $i = 1, 2, \dots, n$, are the roots of the following polynomials:

$$\nu_i(s) = N_i(s) \prod_{\substack{j=1 \\ j \neq i}}^n M_j(s) + \sum_{j=1}^n \left[m_j (l_j s^2 + g) O_{ij}(s) \prod_{\substack{k=1 \\ k \neq i \\ k \neq j}}^n M_k(s) \right] \quad (\text{B6})$$

$$\kappa_i(s) = (M_l l_i - I_{\text{eq}}) s^2 \prod_{\substack{j=1 \\ j \neq i}}^n M_j(s) + \sum_{j=1}^n \left[m_j (l_j s^2 + g) T_{ij}(s) \prod_{\substack{k=1 \\ k \neq i \\ k \neq j}}^n M_k(s) \right] \quad (\text{B7})$$

where $N_i(s)$, $O_{ij}(s)$, and $T_{ij}(s)$ are polynomials defined as follows:

$$N_i(s) = (Al_i + I_{\text{eq}} C_i) s^3 + (Bl_i + I_{\text{eq}} D_i) s^2 + g(A + M_l C_i) s + g(B + M_l D_i) \\ O_{ij}(s) = (l_i C_j - C_i l_j) s^3 + (l_i D_j - D_i l_j) s^2 + g(C_j - C_i) s + g(D_j - D_i) \\ T_{ij}(s) = (l_j - l_i) s^2$$

Appendix C: Proof of the System Stability

Rewrite the equations of motion, Eq. (3), as

$$\left[I_{\text{eq}} + \sum_{i=1}^n m_i q_i^2 \right] \ddot{\theta} - \sum_{i=1}^n m_i l_i \dot{q}_i + \sum_{i=1}^n m_i q_i \dot{q}_i \dot{\theta} + \dot{\theta} \sum_{i=1}^n m_i q_i \dot{q}_i \\ + \left[M_l \sin \theta - \cos \theta \sum_{i=1}^n m_i q_i \right] g = \left[M_l \cos \theta + \sin \theta \sum_{i=1}^n m_i q_i \right] \ddot{u} \quad (\text{C1})$$

$$-m_i l_i \ddot{\theta} + m_i \dot{q}_i - m_i \dot{\theta} q_i \dot{\theta} + k_i q_i - m_i \sin \theta g = -c_i \dot{q}_i - m_i \cos \theta \ddot{u}$$

for $i = 1, 2, \dots, n$

(C2)

We define $\psi = [\theta \quad \mathbf{q}^T]^T$ where $\mathbf{q} = [q_1 \quad q_2 \quad \dots \quad q_n]^T$ as the $(n+1)$ -generalized coordinate vector. Then, the governing equations of motion can be written as

$$\mathbf{M}(\psi) \ddot{\psi} + \mathbf{C}(\psi, \dot{\psi}) \dot{\psi} + \mathbf{G}(\psi) = \mathbf{F} \quad (\text{C3})$$

where $\dot{\psi}$ and $\ddot{\psi}$ are, respectively, the generalized velocities and accelerations vectors, and

$$\begin{aligned} \mathbf{M} &= \begin{bmatrix} I_{eq} + \mathbf{q}^T \mathcal{D}(\mathbf{m}) \mathbf{q} & -\mathbf{l}^T \mathcal{D}(\mathbf{m}) \\ -\mathcal{D}(\mathbf{m}) \mathbf{l} & \mathcal{D}(\mathbf{m}) \end{bmatrix}, \quad \mathbf{C} = \begin{bmatrix} \dot{\mathbf{q}}^T \mathcal{D}(\mathbf{m}) \mathbf{q} & \mathbf{q}^T \mathcal{D}(\mathbf{m}) \dot{\theta} \\ -\mathcal{D}(\mathbf{m}) \mathbf{q} \dot{\theta} & 0 \end{bmatrix} \\ \mathbf{G} &= \begin{bmatrix} G_\theta \\ \mathcal{D}(\mathbf{k}) \mathbf{q} - \mathbf{G}_q \end{bmatrix}, \quad \mathbf{F} = \begin{bmatrix} F_\theta \\ -\mathcal{D}(\mathbf{c}) \dot{\mathbf{q}} - \mathbf{F}_q \end{bmatrix} \end{aligned}$$

where $\mathbf{m} = m_i$, $\mathbf{k} = k_i$, $\mathbf{c} = c_i$ and $\mathbf{l} = l_i$ are the n -vectors of the sloshing masses, spring constants, damping coefficients, and masses distances, respectively, $\mathcal{D}(\mathbf{v})$ is the diagonal matrix of n -vector \mathbf{v} , $G_\theta = M_l g \sin \theta - g \cos \theta \mathbf{m}^T \mathbf{q}$, $\mathbf{G}_q = \mathbf{m} g \sin \theta$, $F_\theta = [M_l \cos \theta + \mathbf{m}^T \mathbf{q} \sin \theta] \ddot{\theta}$, and $\mathbf{F}_q = \mathbf{m} \cos \theta \ddot{\theta}$. It can be shown by direct differentiation and substitution that $\dot{\mathbf{M}} - 2\mathbf{C}$ is a skew symmetric matrix. The equilibrium equations are corresponding to the solution of the following equations:

$$\begin{aligned} \left[M_l \sin \hat{\theta} - \cos \hat{\theta} \sum_{i=1}^n m_i \hat{q}_i \right] g &= \left[M_l \cos \hat{\theta} + \sin \hat{\theta} \sum_{i=1}^n m_i \hat{q}_i \right] \ddot{\theta} \\ k_i \hat{q}_i - m_i g \sin \hat{\theta} &= -m_i \cos \hat{\theta} \ddot{\theta} \quad \text{for } i = 1, 2, \dots, n \end{aligned}$$

To analyze the stability of the system at equilibrium, the following candidate Lyapunov function is considered:

$$V = \frac{1}{2} [\alpha \theta^2 + \mathbf{q}^T \mathcal{D}(\mathbf{k}) \mathbf{q} + \dot{\psi}^T \mathbf{M} \dot{\psi}] \quad (\text{C4})$$

where α is a positive quantity. The time derivative of V is

$$\dot{V} = \alpha \theta \dot{\theta} + \dot{\mathbf{q}}^T \mathcal{D}(\mathbf{k}) \mathbf{q} + \dot{\psi}^T \mathbf{M} \ddot{\psi} + \frac{1}{2} \dot{\psi}^T \dot{\mathbf{M}} \dot{\psi}$$

Using Eq. (C3) and the fact that $\dot{\mathbf{M}} - 2\mathbf{C}$ is a skew symmetric matrix, one can obtain the following:

$$\begin{aligned} \dot{V} &= \alpha \theta \dot{\theta} + \dot{\mathbf{q}}^T \mathcal{D}(\mathbf{k}) \mathbf{q} + \dot{\psi}^T \mathbf{F} - \dot{\psi}^T \mathbf{G} \\ &= \alpha \theta \dot{\theta} + \dot{\mathbf{q}}^T \mathcal{D}(\mathbf{k}) \mathbf{q} + \dot{\theta} F_\theta - \dot{\mathbf{q}}^T \mathbf{F}_q - \dot{\mathbf{q}}^T \mathcal{D}(\mathbf{c}) \dot{\mathbf{q}} \\ &\quad - \dot{\theta} G_\theta - \dot{\mathbf{q}}^T \mathcal{D}(\mathbf{k}) \mathbf{q} + \dot{\mathbf{q}}^T \mathbf{G}_q \\ &= -\dot{\theta} [G_\theta - F_\theta - \alpha \theta] - \dot{\mathbf{q}}^T [\mathbf{F}_q - \mathbf{G}_q + \mathcal{D}(\mathbf{c}) \dot{\mathbf{q}}] \\ &= -\dot{\theta} [G_\theta - F_\theta - \alpha \theta] - \dot{\mathbf{q}}^T [\mathcal{D}(\mathbf{k}) \mathbf{q} + \mathcal{D}(\mathbf{c}) \dot{\mathbf{q}}] \end{aligned}$$

which satisfies $\dot{V} \leq 0$ if $G_\theta - F_\theta > \alpha \theta$. Without loss of generality, the equilibrium is considered at the origin, i.e., $\theta = 0$ and $\hat{q}_i = 0, \forall i$. Therefore, the system is asymptotically stable at the origin based on LaSalle's principle.

References

- [1] Feddema, J. T., Dohrmann, C. R., Parker, G. G., Robinett, R. D., Romero, V. J., and Schmitt, D. J., 1997, "Control for Slosh-Free Motion of an Open Container," *IEEE Control Syst. Mag.*, **17**(1), pp. 29–36.
- [2] Yano, K., and Terashima, K., 2001, "Robust Liquid Container Transfer Control for Complete Sloshing Suppression," *IEEE Trans. Control Syst. Technol.*, **9**(3), pp. 483–493.
- [3] Aboel-Hassan, A., Arafa, M., and Nassef, A., 2009, "Design and Optimization of Input Shapers for Liquid Slosh Suppression," *J. Sound Vib.*, **320**(1–2), pp. 1–15.
- [4] Kaneshige, A., Miyoshi, T., and Terashima, K., 2009, "The Development of an Autonomous Mobile Overhead Crane System for the Liquid Tank Transfer," *IEEE/ASME International Conference on Advanced Intelligent Mechatronics*, Singapore, July 14–17, pp. 630–635.
- [5] Murthy, A. S., Kivila, A., and Singhowe, W., 2012, "Slosh Suppression of a Liquid in a Suspended Container Using Robust Input Shaping," *19th International Congress on Sound and Vibration*, Vilnius, Lithuania, pp. 1–8.
- [6] Pridgen, B., Bai, K., and Singhowe, W., 2013, "Shaping Container Motion for Multimode and Robust Slosh Suppression," *J. Spacecr. Rockets*, **50**(2), pp. 440–448.
- [7] Reyhanoglu, M., and Rubio Hervas, J., 2013, "Nonlinear Modeling and Control of Slosh in Liquid Container Transfer Via a PPR Robot," *Commun. Nonlinear Sci. Numer. Simul.*, **18**(6), pp. 1481–1490.
- [8] AlSaibie, A., and Singhowe, W., 2013, "Experimental Testing of Liquid Slosh Suppression in a Suspended Container With Compound-Pendulum Dynamics," *Ninth Asian Control Conference (ASCC)*, Istanbul, Turkey, June 23–26, pp. 1–6.
- [9] Baozeng, Y., and Lemei, Z., 2014, "Hybrid Control of Liquid-Filled Spacecraft Maneuvers by Dynamic Inversion and Input Shaping," *AIAA J.*, **52**(3), pp. 618–626.
- [10] BiagiottiChiavallini, L., Moriello, D., and Melchiorri, L. C., 2018, "A Plug-in Feed-Forward Control for Sloshing Suppression in Robotic Teleoperation Tasks," *IEEE/RSJ International Conference on Intelligent Robots and Systems (IROS)*, Madrid, Spain, Oct. 1–5, pp. 5855–5860.
- [11] Huang, J., and Zhao, X., 2018, "Control of Three-Dimensional Nonlinear Slosh in Moving Rectangular Containers," *ASME J. Dyn. Syst., Meas., Control*, **140**(8), p. 081016.
- [12] Hasheminejad, S. M., Mohammadi, M., and Jarrahi, M., 2014, "Liquid Sloshing in Partly-Filled Laterally-Excited Circular Tanks Equipped With Baffles," *J. Fluids Struct.*, **44**, pp. 97–114.
- [13] Wang, W., Peng, Y., Zhou, Y., and Zhang, Q., 2016, "Liquid Sloshing in Partly-Filled Laterally-Excited Cylindrical Tanks Equipped With Multi Baffles," *Appl. Ocean Res.*, **59**, pp. 543–563.
- [14] Singer, N. C., and Seering, W. P., 1990, "Preshaping Command Inputs to Reduce System Vibration," *ASME J. Dyn. Syst., Meas., Control*, **112**(1), pp. 76–82.
- [15] Hyde, J. M. S., 1990, "Using Input Command Pre-Shaping to Suppress Multiple Mode Vibration," *IEEE International Conference on Robotics and Automation*, Sacramento, CA, Apr. 9–11.
- [16] Singhowe, W., Seering, W., and Singer, N., 1994, "Residual Vibration Reduction Using Vector Diagrams to Generate Shaped Inputs," *J. Mech. Des.*, **116**(2), pp. 654–659.
- [17] Singhowe, W., Seering, W. P., and Singer, N. C., 1996, "Input Shaping for Vibration Reduction With Specified Insensitivity to Modeling Errors," *Proceedings of the 1996 Japan-USA Symposium on Flexible Automation*, Japan, pp. 307–313.
- [18] Singhowe, W., and Pao, L., 1997, "A Comparison of Input Shaping and Time-Optimal Flexible-Body Control," *Control Eng. Practice*, **5**(4), pp. 459–467.
- [19] Ibrahim, R. A., 2005, *Liquid Sloshing Dynamics: Theory and Applications*, 1st ed., Cambridge University Press, New York.
- [20] Graham, E., and Rodriguez, A., 1952, "Characteristics of Fuel Motion Which Affect Air Plane Dynamics," *ASME J. Appl. Mech.*, **19**, pp. 381–388.
- [21] Disimile, P., and Toy, N., 2019, "The Imaging of Fluid Sloshing Within a Closed Tank Undergoing Oscillations," *Results Eng.*, **2**, p. 100014.
- [22] Abramson, H., N., 1966, "The Dynamic Behavior of Liquids in Moving Containers, With Applications to Space Vehicle Technology," NASA, Washington, DC, Report No. *NASA-SP-106*.